Journal of Nuclear Materials 382 (2008) 1–23

Contents lists available at ScienceDirect

Journal of Nuclear Materials

journal homepage: www.elsevier.com/locate/jnucmat

Irradiation hardening in unalloyed and ODS molybdenum during low dose neutron irradiation at 300 °C and 600 °C

B.V. Cockeram [a,*], R.W. Smith [a], K.J. Leonard [b], T.S. Byun [b], L.L. Snead [b]

[a] Bechtel-Bettis, Inc., P.O. Box 79, West Mifflin, PA 15122-0079, USA
[b] Oak Ridge National Laboratory, P.O. Box 2008, Oak Ridge, TN 37831-6138, USA

ARTICLE INFO

Article history:
Received 31 January 2008
Accepted 13 August 2008

ABSTRACT

Unalloyed molybdenum and oxide dispersion strengthened (ODS) molybdenum were irradiated at 300 °C and 600 °C in HFIR to neutron fluences of 0.2, 2.1, and 24.3 × 10^{24} n/m^2 (E > 0.1 MeV). The size and number density of voids and loops as well as the measured irradiation hardening and electrical resistivity were found to increase sub-linearly with fluence. This supports the idea that the formation of the extended defects that produce irradiation hardening in molybdenum is the result of a nucleation and growth process rather than the formation of sessile defects directly from the displacement damage cascades. This conclusion is further supported by molecular dynamics (MD) simulations of cascade damage. The unalloyed molybdenum had a low impurity interstitial content with less irradiation hardening and lower change in electrical resistivity than is observed for ODS Mo. This result suggests that high-purity can result in slightly improved resistance to irradiation embrittlement in molybdenum at low fluences.
© 2008 Elsevier B.V. All rights reserved.

1. Introduction

Molybdenum is a refractory metal that possesses both high strength and high creep-resistance at elevated temperatures, good thermal conductivity, and measurable tensile ductility at room-temperature [1–5]. The mechanical properties of refractory metals with a body-centered-cubic (bcc) structure, such as molybdenum, are very sensitive to features of the microstructure such as grain size, size and number density of second phases, dislocation density, and concentration of interstitial elements [1–19]. For example, an oxide dispersion strengthened (ODS) molybdenum alloy has exhibited excellent creep-resistance when the material is worked to produce a fine La-oxide dispersion and a fine grain size (≈1.2 μm) [20–23]. The fine grain size and fine oxide dispersion of ODS Mo are also believed to produce high tensile ductility, high fracture toughness, and a low ductile to brittle transition temperature (DBTT) [24–27]. The mechanical properties and DBTT for molybdenum are sensitive to interstitial purity levels. Very low levels of oxygen, and to a lesser extent nitrogen, can result in embrittlement of grain boundaries leading to higher DBTT values [1–3,6–18,28]. Low levels of carbon can mitigate the embrittling effect of oxygen, but carbon contents above 100 ppm can result in less fracture resistance if alloying additions are not present to form carbide precipitates.

Irradiation of commercially available unalloyed molybdenum or molybdenum alloys at temperatures as high as 600 °C generally results in the formation of a high number density (>10^{19}/m^3) of sessile defects that impede dislocation motion and increase the flow stress of the material above the inherent fracture stress promoting brittle failure [27–31]. Irradiation hardening results in embrittlement that is characterized by a substantial increase in the DBTT that can easily exceed 600 °C. In order to design and assess the potential effectiveness of materials modifications by which embrittlement might be mitigated, it is important to question whether the sessile defect clusters are produced directly in the displacement cascade or are formed by a nucleation and growth process. If the formation of defect clusters occurs by a nucleation and growth process, then features of the microstructure and interstitial solute levels that can be controlled and tailored may have a strong effect on irradiation embrittlement via their effect on point defect transport, absorption, and recombination. In contrast, if defects were formed immediately in the damage cascade themselves, material modifications affecting long range point defect behavior would have very little effect on embrittlement. Both experimental studies and molecular dynamics simulations have provided strong evidence for in-cascade defect cluster formation in metals with a face-centered cubic (fcc) structure, such as Ni, Cu, Pt, and Au, and the bcc metal tungsten, but defect clusters in bcc metals with a lower atomic number (iron and vanadium) are formed by a nucleation and growth process [33–36]. Molybdenum has an intermediate atomic number between tungsten and iron, and the propensity for immobile defect formation in the displacement cascade has not been previously investigated. One objective of this work is to provide experimental evidence to determine if loop and void formation occurs in the displacement cascade in molybdenum by

* Corresponding author. Tel.: +1 412 476 5647; fax: +1 412 476 5779.
E-mail address: cockeram@bettis.gov (B.V. Cockeram).

0022-3115/$ - see front matter © 2008 Elsevier B.V. All rights reserved.
doi:10.1016/j.jnucmat.2008.08.052

performing irradiations at 300 °C and 600 °C over a range of low fluences equivalent to 0.011, 0.11, and 1.3 dpa. Molecular dynamics (MD) simulations of displacement damage, employing a Finnis–Sinclair interatomic potential for molybdenum are also reported.

Vacancy diffusion in molybdenum can become prominent at 600 °C and the susceptibility for embrittlement is diminished at temperatures above 600 °C. Since the nucleation and growth of the loops and voids that impede dislocation flow depend on point defect transport kinetics, defect formation can be influenced by pre-existing microstructural sinks and interstitial impurities [3–6,27–32]. The fine grain size and fine oxide particle dispersion of ODS molybdenum has been shown to result in improved resistance to irradiation embrittlement for irradiations at 600 °C exhibiting a DBTT of room-temperature as opposed to 700 °C observed for TZM [27]. The improvement has been attributed to the formation of denuded zones (regions free of extended defects) near grain boundaries that allow the ductile–laminate toughening mechanism to operate [27]. For irradiations at 300 °C the width of the denuded zones is negligible, and the tensile DBTT for ODS Mo is identical to values of about 800 °C obtained from commercially available low carbon arc cast (LCAC) molybdenum and TZM [27]. A fine grain size and lower interstitial levels have also been shown to result in slightly lower DBTT values for LCAC Mo with a DBTT of 300 °C observed for 600 °C irradiations, as compared to 700 °C for commercially available TZM [32]. Low DBTT values of room-temperature have been reported for unalloyed molybdenum that contains low interstitial levels (30 ppm carbon and 5 ppm oxygen) and has a fine grain size of 2 μm for irradiations at 373 °C, 519 °C, and 600 °C, although brittle behavior was observed in this experiment for irradiations at 406 °C [28]. A second purpose of this work is to understand the role of fine grain size, fine oxide particles, dislocation density, and purity on the mitigation of irradiation embrittlement by the irradiation of as-worked ODS molybdenum and as-worked unalloyed molybdenum that has been purified to lower the carbon and oxygen content.

2. Materials and experimental procedure

Wrought ODS Molybdenum plate (6.35 mm thick) was obtained from H.C. Starck, Inc. with the composition provided in Table 1 [24–26]. The processing of ODS molybdenum has been described elsewhere [20–27], and consists of wet doping Mo-oxide (MoO_2) powder with a La-nitrate ($La(NO_3)_3 \cdot 6H_2O$) aqueous solution, pyrolyzing to form a fine dispersion of La-oxide (nominally La_2O_3) in molybdenum powder, consolidation and wrought processing into plate. This was followed by warm rolling to sheet (0.62 mm thick) by heating in hydrogen to temperatures between 1600 °C and 500 °C in reduction steps of 10%. The high-purity molybdenum (HP-LCAC) was produced by heating LCAC Mo plate [37] (6.35 mm thick) obtained from H.C. Starck in hydrogen at 1600 °C for 72 h for purification. The annealed plates were welded together to form an electrode, melted using a vacuum arc AC melting process into a 5.08 cm diameter ingot, and dynapak extruded into a 1.27 cm thick bar after heating to 1400 °C (in hydrogen) at a pressure of 75.8 MPa. The bar was rolled into 0.66 mm sheet at temperatures between 1400 °C and 500 °C in steps of 10% reduction by pre-heating in hydrogen at Pittsburgh Materials Technology Inc. (PMTI), Large, PA. The rolling at 500 °C produced an estimated 28% cold work for ODS Mo and 68% cold work for HP-LCAC.

Sub-sized SS-1 flat tensile specimens were machined from the as-worked sheets in the longitudinal orientation with a nominal size of 44.45 mm long × 4.95 mm wide with a 20.32 × 1.52 mm gauge length and nominal thickness of 0.51 mm [24–27,31,32,38]. The tensile specimens were tested either in the longitudinal as-worked (LAW) condition or after a vacuum heat treatment at 1200 °C/1 h for ODS or 800 °C/1 h for HP-LCAC (longitudinal stress-relieved (LSR) condition). All specimens were laser scribed for identification and electropolished.

Capsule designs identical to those described in previous work were used to irradiate the tensile specimens at nominal temperatures of 300 °C and 600 °C [27,31,32,38]. Thermal calculations show that the maximum temperature gradients through the tensile specimens were 10 °C and 15 °C for the radial and axial direction, respectively, at a target irradiation temperature of 300 °C and on the order of 25 °C in either direction for the 600 °C irradiation temperature. Analysis of passive silicon carbide temperature monitors by measuring electrical resistivity following isochronal annealing [39] indicated that the irradiation temperature was within a range of 5–74 °C of the target irradiation temperatures reported in Table 2. Irradiations of two of the capsules (BS3 and BS6) were performed in the peripheral target tube position (PTP) of the high flux isotope reactor (HFIR) in two cycles at 85 MW of power (Table 2). The other four capsules were irradiated at the same position at equivalent fluxes in the hydraulic tube of HFIR for times of 6.7 h and 69.7–70.1 h at nominal irradiation temperatures of 300 °C (BS-1 and BS-2) and 600 °C (BS-4 and BS-5). No effort was made to shield the capsules from the spectrum produced by HFIR, which has an estimated nominal peak fast flux of 1×10^{19} n/m^2 s ($E > 0.1$ MeV) and a peak thermal flux of 2.2×10^{19} n/m^2 s ($E < 0.1$ MeV) [27,31,32,38]. The fast neutron fluxes are very similar for the two positions (8.4 and 8.9×10^{18} n/m^2 s ($E > 0.1$ MeV)). The ratio of fast flux to thermal flux is relatively constant in HFIR for these positions.

The differences in calculated temperature for the BS-1, BS-2, and BS-3 capsules was generally within the range of temperatures previously identified as being close to 300 °C [27,31,32,38] and the variation in average capsule temperature (252–309 °C) was 57 °C. This suggests the capsule temperature for BS-1, BS-2, and BS-3 was close enough to previous results for 300 °C that the nominal capsule temperature can be assumed to be 300 °C. For the irradiation of capsules BS-4, BS-5, and BS-6, the nominal temperatures (628–674 °C) are slightly higher than reported for irradiations at nominally 600 °C (560–609 °C) [27,31,32,38]. The temperatures

Table 1
Chemical analysis of the LAW ODS Mo rolled from sheet and purified LCAC (HP-LCAC) molybdenum, as provided in material certification reports and determined using combustion and GDMS analysis. Unless noted, all compositions given in wt% ppm

Material/Lot#	C	O	N	Ti	Zr	Fe	Ni	Si	La	Al	Ca	Cr	Cu	Other
ODS Molybdenum/Ingot #382 Heat# LA22963	10	NA	NA	<10	NA	74	12	24	1.6 wt%	21	320	24	10	<10 Mg <10 Mn <10 Pb <10 Sn
High-Purity LCAC (HP-LCAC) Molybdenum/Heat# M1529	20	4	3	5	1	20	3	3	0.6	1	0.07	3	0.4	120 W 14 Nb

Notes:
(1) NA = not available.
(2) The ODS and LCAC starting material were obtained from H.C. Starck, Cleveland, OH.
(3) Trace GDMS composition for elements not listed was <1 ppm.

Table 2
Summary of the irradiation conditions for LAW high-purity LCAC molybdenum (HP-LCAC) and LAW ODS sheet rolled from plate

Irradiation capsule	Design specimen irradiation temperature °C [°F]	True irradiation temperature for temperature monitor analysis (°C)	HFIR cycle number	Neutron flux [$\times 10^{18}$ n/m^2 s, $E > 0.1$ MeV]	Neutron fluence [$\times 10^{24}$ n/m^2, $E > 0.1$ MeV]	Neutron fluence, molybdenum dpa
BS1	300	331 ± 20	407	8.4	0.2	0.011
BS2	300	291 ± 20	407	8.4	2.1	0.11
BS3	300	253 ± 20	403A&404	8.9	24.3	1.29
BS4	600	653 ± 10	407	8.4	0.2	0.011
BS5	600	640 ± 10	407	8.4	2.1	0.11
BS6	600	674 ± 20	403A&404	8.9	24.3	1.29

Notes:
(1) The target irradiation temperature was the calculated tensile specimen temperature objective for the irradiation test. The irradiation temperatures were generally within ±50 °C for irradiations at 300 °C and 600 °C.
(2) The conversion from neutron fluence to molybdenum dpa for the HFIR spectrum was determined using the code SPECTER [41].
(3) These irradiations were performed over a period of 27 March 2005 to 6 January 2006. Cycles 403A and 404 were used to produce a neutron fluence of 24.3 $\times$ 10^{24} n/m^2 in position #5 of the PTP locations for capsules BS3 and BS6. Capsules BS1, BS2, BS4, and BS5 were irradiated in the Position #6 in cycle 407 in the hydraulic tube. The MW days and hours of operation for each capsule and cycle are as follows: capsules BS3 and BS6 in cycles 403A and 404 (2690.3 MW days and 759.6 h), capsule BS1 in cycle 407 (23.7 MW days and 6.7 h), capsule BS2 in cycle 407 (248.3 MW days and 70.1 h), capsule BS4 in cycle 407 (23.7 MW days and 6.7 h), capsule BS5 in cycle 407 (246.9 MW days and 69.7 h).
(4) Actual specimen irradiation temperatures were determined from analysis of the temperature monitors.

are close enough to the values from previous irradiations that the nominal irradiation temperature for capsules BS-4, BS-5, and BS-6 is assumed to be nominally 600 °C.

The displacement damage produced by irradiation was determined to be primarily the result of the fast flux. The dpa values calculated in Table 2 for these irradiations included contributions from both the fast and thermal flux. The fast flux and dpa rate for both the PTP and hydraulic tube positions are comparable. The maximum dose values shown in Table 2 (0.011–1.3 dpa [41]) are expected to produce very low concentrations of transmutation products (<0.2 wt%) that are primarily Tc and Ru with 3–4 ppm amounts of Zr and Nb [27,31,32,38,40]. The low levels of transmutation products produced at these low fluences are believed to have little effect on the mechanical properties compared to the defects (voids/loops) produced by irradiation [27,31,32,38,40].

Tensile tests were performed at temperatures ranging from −196 °C to 600 °C at an actuator displacement rate of 0.017 mm/s (strain rate = 0.00083 min^{-1}) in accordance with ASTM E8 [42] using methods previously described [27,31,32]. Engineering stress–strain values were determined from the load and crosshead displacement record, and no correction was made for the compliance of the load train for the stress–strain curves [27]. Strain hardening exponents were determined from true stress–strain plots of data calculated from the engineering stress–strain values. Room-temperature tests were conducted at atmospheric pressure, and testing at elevated temperatures was performed in a vacuum furnace (<6 $\times$ 10^{-5} MPa) with a 30 min soak time prior to testing. Sub-ambient temperature testing was accomplished using nitrogen gas from a liquid nitrogen boil-off to cool [27]. Fractographic examinations were performed using a Scanning Electron Microscope (SEM). Prior to tensile testing pre- and post-irradiation electrical resistivity measurements were made on the same specimen using a standard 4-point procedure [38,43].

Hardness measurements were performed on representative unirradiated and irradiated tensile specimens using a Buehler Microhardness tester with a Vicker's tip at a 500 g load with a 5 s dwell time [38]. Discs 3 mm in diameter were punched from the tab section of the tensile specimens for transmission electron microscopy (TEM). The TEM discs were prepared by mechanical polishing followed by electropolishing using a 13 vol.% H_2SO_4 in methanol solution at −10 °C (250–270 mA, 21–22 V), similar to that of [44]. Samples were examined in a CM200-FEG instrument

Table 3
Summary of non-irradiated tensile data for unalloyed HP-LCAC molybdenum in the longitudinal orientation for the as-worked and stress-relieved condition

Test temperature (°C)	Tensile strength (MPa)		Tensile ductility (%)			Strain hardening exponent, n
	Ultimate tensile stress	0.2% Yield stress	Total elongation	Uniform elongation	Reduction in area	
Longitudinal as-worked data						
−192	1444.5	NA	<1	0	15	–
−153	1512.1	1499.0	3	2	19	–
−151	1496.2	1398.3	2	2	13	–
−103	1313.5	1267.3	5	4	42	–
−102	1343.8	1239.7	5	3	38	–
−100	1348.0	1308.7	3.9	0.9	–	0.005
−53	1128.0	1052.9	8	7	42	–
−50	1192.1	1121.1	4.2	1.0	–	0.041
26	943.2	858.4	5	4	45	–
450	741.9	690.9	3.2	1.1	–	0.132
600	612.3	526.1	3.6	1.1	–	0.142
Longitudinal stress-relieved data						
−193	1423.8	NA	<1	0	3	–
−151	1416.2	1403.8	3	2	36	–
−151	1410.0	1385.2	3	2	27	–
−104	1200.4	1174.9	6	4	38	–
−101	1158.4	1117.7	6	5	43	–
−52	1056.3	968.7	7	5	50	–
26	766.7	702.6	13	12	54	–

Each line represents a single test result.
Note: '–' means that a value was not measured for this condition.

at ORNL, with defect damage in the samples analyzed at several locations in each sample using two-beam and weak beam imaging conditions with images collected over a large range of magnifications. Thickness measurements from each viewed location were performed using the Kossel–Möllenstedt fringe spacing technique in the zero order Laue zone convergent beam electron diffraction pattern taken under the $g = 110$ two-beam condition.

Molecular dynamics simulations were conducted using a parallel version of the MDCASK program supplied by the Lawrence Livermore National Laboratory [45]. Displacement cascades are simulated by selecting an atom near the center of the computational cell to become a primary knock-on atom (PKA) and imparting to it some amount of kinetic energy at the start of the MD simulation. In the present investigation, cascades were tracked for a duration of roughly 10 ps. PKA energies of 1, 2, 5, 10, 20 and 40 keV were used and the PKA direction was taken as [1 3 5] in the BCC Mo lattice. Prior to the introduction of the PKA, the computational cells were first equilibrated to an ambient temperature of either 25 °C, 300 °C, or 650 °C. Equilibration was done using the velocity scaling algorithm in MDCASK. Three-dimensional periodic boundary conditions were applied to the computational cells and the cell dimensions were scaled to account for thermal expansion. Computational cell size was selected in accordance with previous work done on other systems [46,47] and to minimize any size effect that would result from temperature increases due to the dissipation of the PKA's kinetic energy. In order to improve statistics, five simulations were run at each PKA energy and cell temperature. The interatomic potential used to describe the Mo system was constructed by joining together the Universal potential [48] at short range with a Finnis–Sinclair potential previously fit to equilibrium properties of Mo [49]. The connection was made with an exponential blend designed to maintain the continuity of energy and first derivative at the junction to both the Universal and Finnis–Sinclair regimes [50].

3. Results and discussion

3.1. Non-irradiated tensile properties

Tensile properties for non-irradiated LAW HP-LCAC and ODS Mo are summarized in Tables 3 and 4, respectively. The microstructure of HP-LCAC and ODS sheet is shown in Fig. 1 to consist of elongated, sheet-like pancaked grains that are similar in appearance to commercially produced LCAC, ODS, and TZM Mo flat products

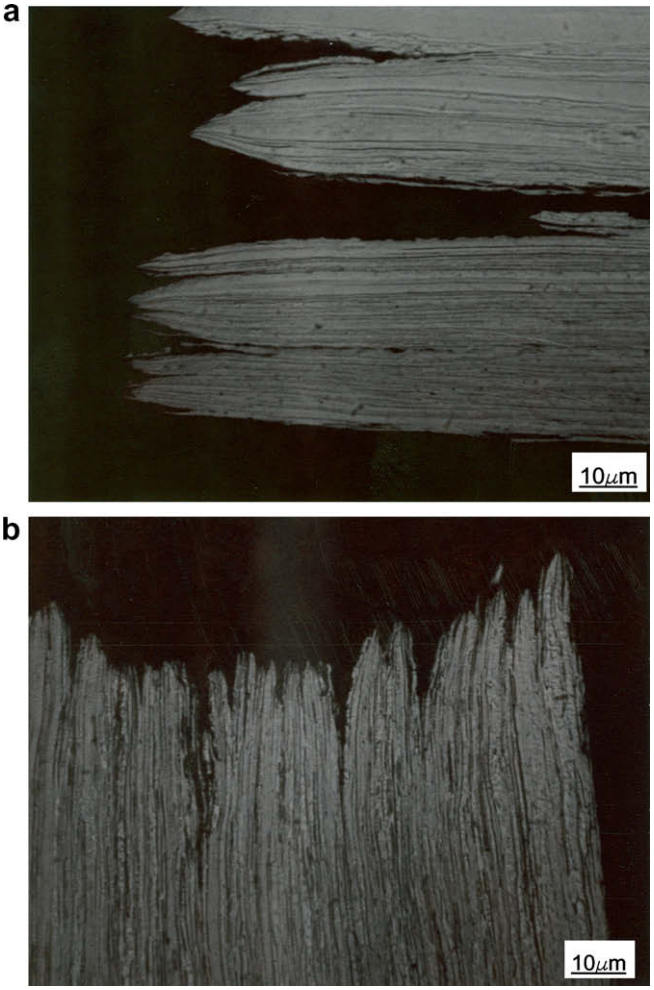

Fig. 1. Optical metallography at the fracture surface of a non-irradiated tensile specimen in the longitudinal orientation that was tested at a temperature above the DBTT: (a) unalloyed HP-LCAC molybdenum tested at −50 °C, and (b) LAW ODS molybdenum tested at −50 °C.

Table 4
Summary of non-irradiated tensile data for ODS molybdenum sheet rolled from plate in the longitudinal orientation for the as-worked and stress-relieved condition

Test temperature (°C)	Tensile strength (MPa)		Tensile ductility (%)			Strain hardening exponent, *n*
	Ultimate tensile stress	0.2% Yield stress	Total elongation	Uniform elongation	Reduction in area	
Longitudinal as-worked data						
−195	1518.3	1521.0	<1	0	0	–
−195	1040.5	NA	0	0	0	–
−149	1285.9	1272.8	3	3	38	–
−101	1321.1	1250.1	10	7	36	–
−100	1279.0	1259.0	6.8	1.6	–	0.025
−49	1009.4	966.7	11	9	45	–
25	799.8	741.2	14	12	58	–
99	658.5	564.0	9	7	65	–
300	677.8	659.9	4.0	1.4	–	0.039
302	560.6	489.5	4	2	69	–
Longitudinal stress-relieved data						
−195	1849.2	1823.7	<1	<1	2	–
−150	1372.8	1359.7	2	1	31	–
−102	1243.9	1159.7	7	5	37	–
−50	1063.2	1024.6	12	11	43	–
25	883.9	816.4	7	6	58	–
97	729.5	702.6	6	4	61	–
302	630.2	610.9	3	1	69	–

Note: '–' means that a value was not measured for this condition.

[24–27,31,32]. The lower rolling temperatures (500 °C) used to produce the LAW HP-LCAC and LAW ODS Mo are shown in Table 5 to result in grains that are slightly thinner and longer than for commercially produced LCAC and LSR ODS Mo.

Table 5
Summary of grain size measurements for wrought unalloyed HP-LCAC Mo sheet and ODS sheet rolled from plate

Alloy	Grain diameter (μm)		Grain length (μm)	
	Average	Standard deviation	Average	Standard deviation
Unalloyed Mo Sheet – LAW	1.3	0.9	452	317
Unalloyed Mo Sheet – LSR	1.3	0.8	383	181
[a]LCAC Sheet – LSR	3.9	2.5	172	79
[a]LCAC Sheet – TSR	5.0	2.7	78.1	38.2
[b]ODS Sheet – LSR	1.2	0.8	45.7	25.0
[b]ODS Sheet – TSR	2.5	1.0	33.3	12.1
[b]ODS Plate – LSR	1.4	0.7	29.0	16.2
[b]ODS Plate – TSR	2.0	1.1	13.6	6.6
ODS Sheet from plate – LAW	0.9	0.4	221	159
ODS Sheet from plate – LSR	0.8	0.4	285	159

Values for wrought LCAC sheet and ODS plate are also reported.
[a] Results for LCAC are reported in [31].
[b] Results for ODS Sheet and Plate are reported in [24,27].

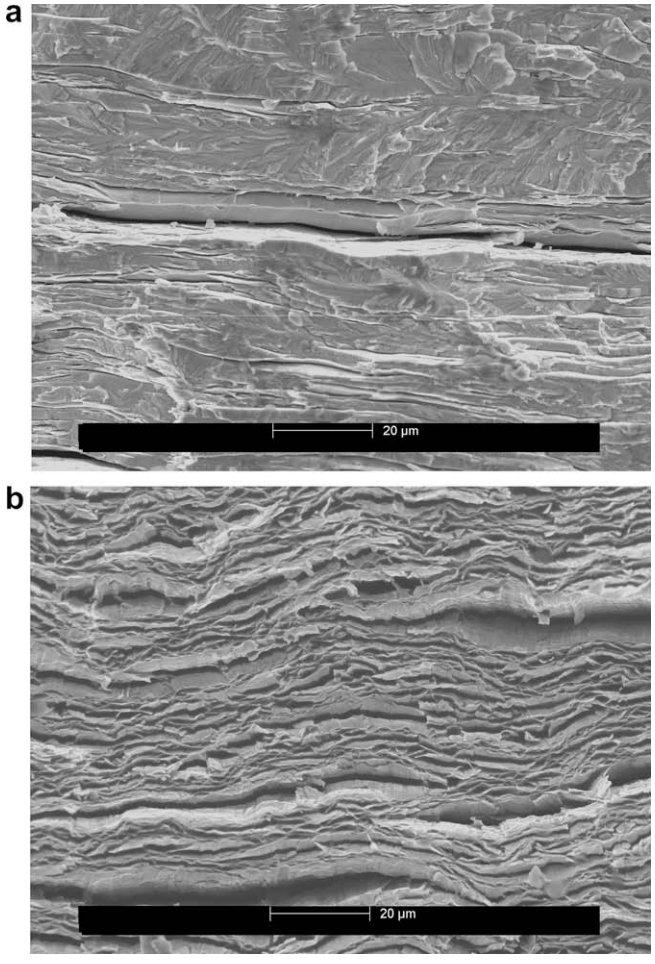

Fig. 2. SEM Fractography from the fracture surface of a non-irradiated LAW tensile specimens tested at a temperature near the DBTT: (a) unalloyed HP-LCAC molybdenum tested at −150 °C, and (b) LAW ODS molybdenum tested at −150 °C.

Fig. 2 shows that LAW HP-LCAC and LAW ODS Mo exhibit a ductile-laminate failure mode at temperatures equal to or greater than the DBTT, which is −150 °C for both materials in the LAW and LSR condition (Table 6). Measurable ductility and plasticity in the stress–strain curves are observed at temperatures equal to or higher than the DBTT. The ductile–laminate failure mode results from fracture initiation at grain boundaries between the sheet-like grains that leaves grain ligaments that are stretched to failure with a high degree of plasticity [24–27,51,52]. Linear-elastic stress–strain curves, low plasticity, and brittle cleavage across grains are observed at temperatures below the DBTT (−194 °C). This indicates that the DBTT for HP-LCAC and LAW ODS was higher than −194 °C and lower than −150 °C, but is conservatively defined as −150 °C for both materials, see Table 6. The finer grain size and higher dislocation density for LAW HP-LCAC-Mo and LAW ODS results in slightly higher tensile strengths, higher ductility at lower temperatures, and slightly lower non-irradiated DBTT values compared to commercially available LSR LCAC and ODS molybdenum. The lowest tensile strength values observed for HP-LCAC are likely the result of the lower interstitial content. Slightly higher tensile strength values are generally observed for the respective LAW versions of HP-LCAC and ODS in comparison to the LSR condition, which can be attributed to the higher dislocation density. However, the differences in tensile strength between the LAW and LSR condition was not significant, which suggests the strength of molybdenum is not a strong function of initial dislocation density.

The stress–strain curves for LAW HP-LCAC and LAW ODS Mo shown in Fig. 3 indicate low strain hardening exponents of $n = 0.142–0.005$ (Tables 3 and 4) are observed that are consistent with the literature data for commercial molybdenum alloys [8–19,24–32,53–61]. The stress–strain data were determined from the raw load–displacement results, and no correction was made for the compliance of the load frame. LSR LCAC and LSR ODS sheet exhibit a slight separation of upper and lower yield points at sub-ambient temperatures [24–32], but distinct upper and lower yield points are not observed for LAW HP-LCAC and LAW ODS in Fig. 3. The appearance of the upper and lower yield points in LSR LCAC, HP-LCAC, and ODS likely results from the lower initial dislocation density and lack of dislocation sources resulting in a higher stress to create mobile dislocations than needed to move the dislocations required to support plastic deformation. The higher dislocation density in LAW HP-LCAC and LAW ODS Mo likely results in the presence of more dislocation sources or creates barriers to dislocation motion so that the stress for dislocation movement

Table 6
Summary of pre- and post-irradiation DBTT values determined from tensile testing for HP-LCAC Mo and LAW ODS Mo rolled from plate for the in-cascade irradiations

Material	Pre-irradiation DBTT	Post-irradiation DBTT at three fluences [n/m^2, $E > 0.1$ MeV]		
		0.2×10^{24}	2.1×10^{24}	24.3×10^{24}
300 °C Irradiations				
Unalloyed Mo HP-LCAC Sheet/LAW	−150 °C	−150 °C	−150 °C	450 °C
Unalloyed Mo HP-LCAC Sheet/LSR	−150 °C	–	–	–
ODS Sheet/LAW	−150 °C	−150 °C	23 °C	450 °C
ODS Sheet/LSR	−150 °C	–	–	–
600 °C Irradiations				
Unalloyed Mo HP-LCAC Sheet/LAW	−150 °C	−150 °C	−150 °C	−50 °C
Unalloyed Mo HP-LCAC Sheet/LSR	−150 °C	–	–	–
ODS Sheet/LAW	−150 °C	−150 °C	−150 °C	−50 °C
ODS Sheet/LSR	−150 °C	–	–	–

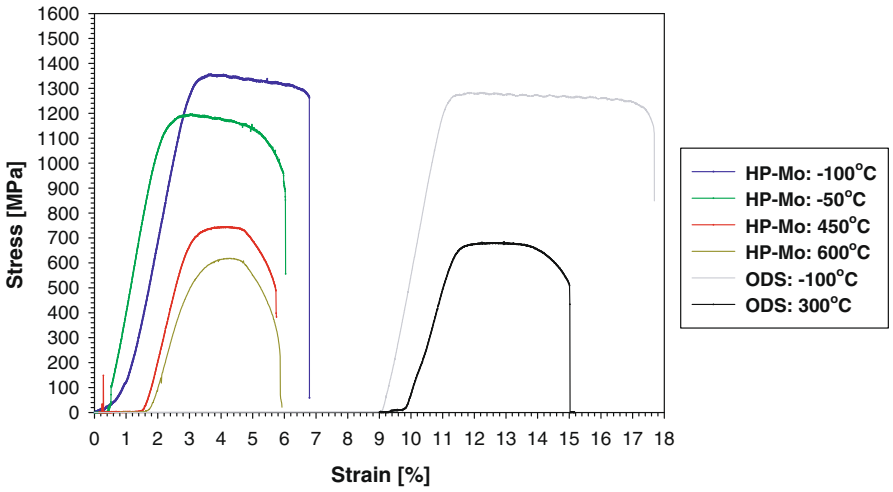

Material	HP-LCAC-Mo				ODS Mo	
Test Temperature	-100 °C	-50 °C	450 °C	600 °C	-100 °C	300 °C
n	0.005	0.041	0.132	0.142	0.025	0.039

Fig. 3. Stress–strain curves for non-irradiated LAW HP-LCAC and LAW ODS Mo sheet. Strain hardening exponent results are also provided.

and dislocation source activation are more comparable and upper/lower yield points are not observed.

3.2. Post-irradiation tensile and hardness for irradiations at nominally 300 °C

Fig. 4 shows that for irradiations at nominally 300 °C to the higher fluence of 24.3×10^{24} n/m^2, LAW HP-LCAC and LAW ODS all exhibit plasticity in the stress–strain curves (Fig. 5), and low amounts of total elongation (0.4–1.5%, see Tables 7 and 8). The stress–strain data were determined from the raw load-displacement results for the testing of all irradiated materials, and no correction was made for the compliance of the load frame. Higher reduction in area (RA) values (26–27%) and mixed-mode fractures with local ductile-laminate failure were observed following tensile testing at 450 °C and 600 °C in Fig. 6. In all cases where plasticity is observed in the stress–strain curves, prompt yielding occurs with a very low uniform elongation and negative strain hardening exponent that is typical of results for irradiated materials [27–36]. Linear-elastic stress–strain curves, no ductility, and a mixed-mode failure with primarily cleavage were observed for both alloys at 300 °C. This indicates that the DBTT for LAW HP-LCAC and LAW ODS Mo was between 450 °C and 300 °C, but is conservatively defined as 450 °C (Table 6). Previous 300 °C irradiations of commercially available molybdenum alloys, such as LSR LCAC and LSR ODS have resulted in a tensile DBTT between 600 °C and 800 °C for irradiations to higher and lower fluences, see Figs. 7 and 8. Although LAW HP-LCAC and LAW ODS Mo have not been irradiated to the exact fluence conditions achieved for LSR LCAC and LSR ODS, some improvement is observed for LAW HP-LCAC and LAW ODS Mo with a slightly lower DBTT.

For irradiations of LAW HP-LCAC at 300 °C to lower fluences of 2.1 and 0.2×10^{24} n/m^2 and LAW ODS at the lowest fluence of 0.2×10^{24} n/m^2, plasticity in the stress–strain curves, measurable levels of elongation (0.6–5.1%) and RA (2–47%), and a mixed-mode failure with local ductile–laminate features were observed at test temperature of −150 °C, room-temperature and 300 °C. This indicates the DBTT for LAW HP-LCAC and LAW ODS Mo at these lower fluences is below −150 °C and is conservatively defined as −150 °C, which is unchanged from the non-irradiated condition (Table 6). For LAW ODS irradiated at 300 °C to a fluence of 2.1×10^{24} n/m^2, plasticity in the stress–strain curves, measurable ductility (0.3–1.1% elongation and 39% RA), and ductile-laminate failure modes are observed at room-temperature and 300 °C, while linear-elastic stress–strain curves, low ductility, and brittle failure modes are observed at −150 °C. This indicates that the DBTT for LAW ODS at a fluence of 2.1×10^{24} n/m^2 was between −150 °C and room-temperature, and is conservatively defined as room-temperature.

In addition to the lower DBTT values observed for HP-LCAC at the lower fluence, the tensile strength and irradiation hardening values for LAW HP-LCAC Mo are shown in Fig. 7 to be lower than for LAW ODS Mo at the highest fluence (24.3×10^{24} n/m^2) and reported values for LSR LCAC irradiated to even a lower fluence of 10.5×10^{24} n/m^2 [31]. Irradiation hardening is reflected here as the difference between the post-irradiated and pre-irradiated tensile strength values. Because fracture occurs prior to yielding at test temperatures below the DBTT, a true measure of irradiation hardening cannot be made because the post-irradiated yield stress is not reached. Thus, fracture stress can be taken as a lower bound measure of irradiation hardening and is subject to the inherent data scatter normally associated with the strength measurement of brittle materials.

A large increase in tensile strength for the 300 °C irradiations is observed at the lowest fluence of 0.2×10^{24} n/m^2, but the largest increase in tensile strength and irradiation hardening is observed between a fluence of 0.2–2.1×10^{24} n/cm^2. Although the tensile strength and irradiation hardening values for LAW ODS Mo were slightly higher than LAW HP-LCAC Mo at the highest fluence of 24.3×10^{24} n/m^2, the irradiation hardening for LAW ODS was comparable to HP-LCAC at the intermediate fluence (2.1×10^{24} n/m^2), and lower than HP-LCAC at the lowest fluence of 0.2×10^{24} n/m^2. The slightly lower DBTT and irradiation hardening for LAW ODS and LAW HP-LCAC Mo compared to LSR LCAC indicate the presence of a fine grain size with fine particles and higher dislocation density (LAW ODS) and higher dislocation density and higher purity (LAW HP-LCAC) provides some improved resistance to irradiation embrittlement for 300 °C irradiations to a highest fluence of

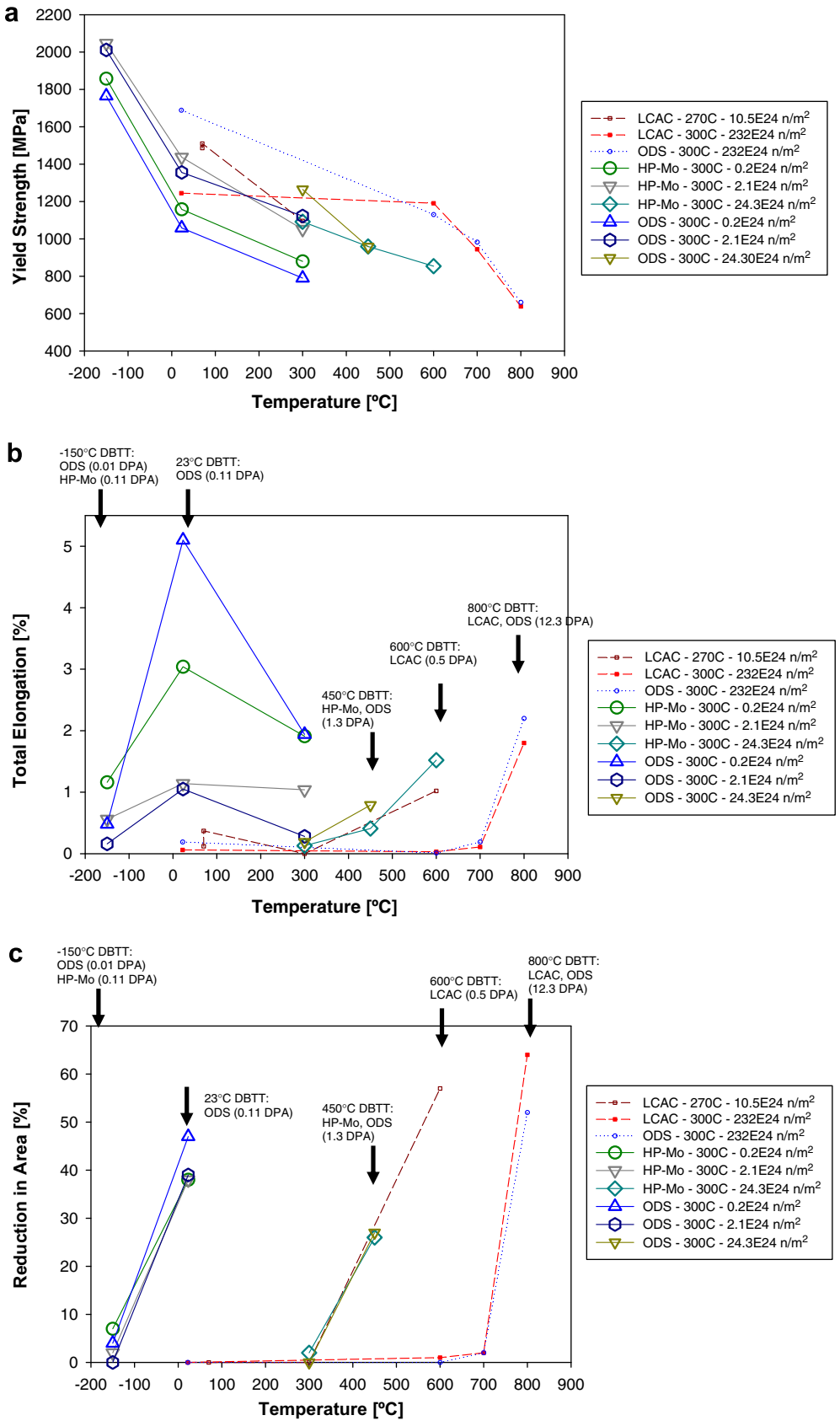

Fig. 4. Comparison of post-irradiated tensile data for LAW HP-LCAC and LAW ODS Mo sheet that was irradiated in HFIR at nominally 300 °C to fluences of 0.2, 2.1, and 24.3×10^{24} n/m^2 with previously reported results for LSR LCAC and LSR ODS Mo [27,31,32]: (a) 0.2% yield strength, (b) total elongation, and (c) reduction in area.

24.3×10^{24} n/m^2. The lowest increase in tensile strength, irradiation hardening and lower DBTT values at lower fluence for LAW HP-LCAC Mo indicates that high-purity provides slightly better resistance to embrittlement.

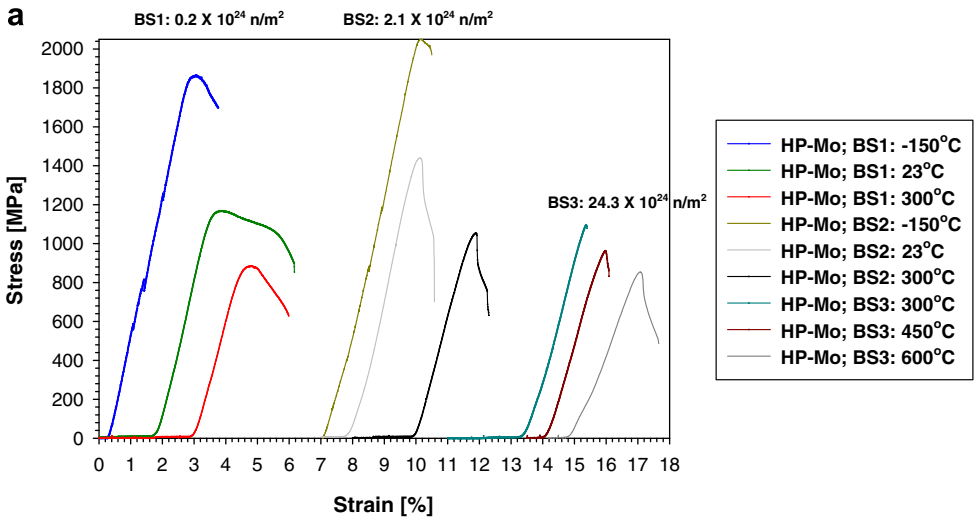

Capsule	BS1			BS2			BS3		
Test Temp	-150 °C	23 °C	300 °C	-150 °C	23 °C	300 °C	300 °C	450 °C	600 °C
N	-0.029	-0.259	-0.830	-0.082	-2.14	-2.97	--	-0.536	-2.94

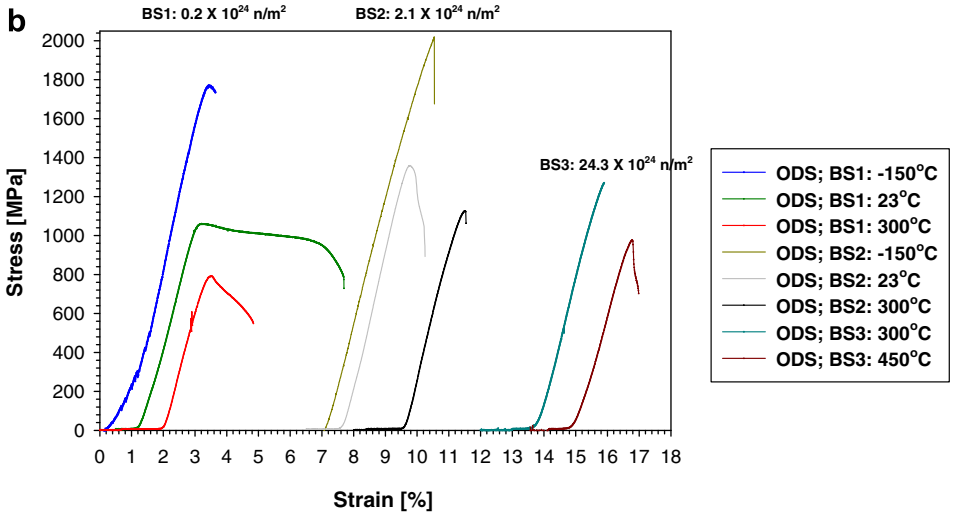

Capsule	BS1			BS2			BS3	
Test Temp	-150 °C	23 °C	300 °C	-150 °C	23 °C	300 °C	300 °C	450 °C
N	0.241	-0.070	-0.814	--	-1.59	-0.843	--	-4.68

Fig. 5. Stress–strain curves for LAW High-Purity LCAC (HP-LCAC) molybdenum and LAW ODS molybdenum specimens that were irradiated in HFIR at nominally 300 °C in capsules BS-1, BS-2, and BS-3 to nominal fluences of 0.2, 2.1, and 24.3 × 10^{24} n/m^2 (E > 0.1 MeV), respectively: (a) HP-LCAC, and (b) LAW ODS. Strain hardening exponent results are also provided below and in Tables 7 and 8.

3.3. Post-irradiation tensile and hardness for irradiations at nominally 600 °C

Considering the irradiations at nominally 600 °C to the higher dose of 24.3 × 10^{24} n/m^2, LAW HP-LCAC and LAW ODS Mo are shown in Figs. 9 and 10 to exhibit plasticity in the stress–strain curves, measurable ductility (0.4–2.6% total elongation and 2–7% RA, see Tables 7 and 8). Mixed-mode failures with localized ductile-laminate failures were observed following tensile testing at −50 °C and room-temperature (Fig. 11). Prompt yielding with low uniform elongation and negative strain hardening exponents were generally observed in the stress–strain curves when ductile behavior is exhibited, consistent with tensile results for other irradiated metals [27–36]. Linear-elastic behavior in the stress–strain curves, no ductility, and a brittle failure mode were observed for the testing of LAW HP-LCAC and LAW ODS at −100 °C. This indicates that the DBTT for LAW HP-LCAC and LAW ODS Mo was between −50 °C and −100 °C, but is conservatively defined as -50 °C (Table 6). This result is significant because previous irradiations of commercially available molybdenum alloys, such as LSR LCAC and LSR TZM, at 600 °C to higher fluences of 27.0, 72.6, and 246 × 10^{24} n/m^2 have resulted in tensile DBTT values between 300 °C and 700 °C [31,32], see Fig. 8. The DBTT of −50 °C observed for LAW HP-LCAC and LAW ODS Mo is an improvement

Table 7
Summary of irradiated tensile data for LAW HP-LCAC molybdenum sheet

Nominal irradiation temperature (°C)/capsule	Neutron fluence (n/m^2), [E > 0.1 MeV]	Test temperature (°C)	Tensile strength (MPa)		Tensile ductility (%)			Strain hardening exponent, n
			Ultimate tensile stress	0.2% Yield stress	Total elongation	Uniform elongation	Reduction in area	
300/BS1	0.2×10^{24}	−150	1861.0	1857.5	1.16	0.26	7	−0.029
		RT	1165.3	1158.4	3.04	0.45	38	−0.259
		300	882.6	879.8	1.91	0.33	–	−0.830
300/BS2	2.1×10^{24}	−150	2047.1	2047.1	0.56	0.11	2	−0.082
		RT	1436.9	1436.9	1.14	0.22	38	−2.14
		300	1051.5	1051.5	1.04	0.22	–	−2.97
300/BS3	24.3×10^{24}	300	1092.2	1092.2[1,2]	0.13	0.09	2	–
		450	959.1	959.1	0.41	0.15	26	−0.536
		600	853.6	853.6	1.52	0.13	–	−2.94
600/BS4	0.2×10^{24}	−196	1880.3	1880.3[1,2]	0.15	0.15	0	–
		−150	1580.3	1572.1	2.19	0.29	3	−0.110
		−100	1427.3	1417.6	2.79	0.50	–	−0.099
600/BS5	2.1×10^{24}	−196	1890.6	1890.6[1,2]	0.07	0.07	0	–
		−150	1676.9	1673.4	1.49	0.43	4	−0.110
		−100	1414.2	1403.1	5.92	0.71	–	0.009
600/BS6	24.3×10^{24}	−100	1518.3	1518.3[1,2]	0.14	0.14	0	–
		−50	1330.7	1320.4	0.49	0.49	2	0.314
		RT	1132.2	1069.4	2.60	1.23	–	0.135

Notes:
(1) Since the uniform elongation was <0.2%, the yield strength cannot be determined, and is listed as being equal to the ultimate strength.
(2) Prompt brittle fracture was observed with a slight amount of yielding at stresses near the yield point.
(3) Initial fracture at pinhole followed by a second test shoulder loading. Results are reported for the shoulder loading test.
(4) '–' means that a value was not measured for this condition.
(5) RT = room-temperature.

Table 8
Summary of irradiated tensile data for LAW ODS molybdenum rolled into sheet from plate

Nominal irradiation temperature (°C)/capsule	Neutron fluence (n/m^2), [E > 0.1 MeV]	Test temperature (°C)	Tensile strength (MPa)		Tensile ductility [%]			Strain hardening exponent, n
			Ultimate tensile stress	0.2% Yield stress	Total elongation	Uniform elongation	Reduction in area	
300/BS1	0.2×10^{24}	−150	1765.1	1765.1	0.48	0.26	4	0.241
		RT	1058.4	1058.4	5.10	0.28	47	−0.070
		300	790.2	790.2	1.94	0.24	–	−0.814
300/BS2	2.1×10^{24}	−150	2011.3	2011.3[1,2,3]	0.16	0.16	0	–
		RT	1355.6	1355.6	1.05	0.21	39	−1.59
		300	1122.5	1122.5	0.28	0.26	–	−0.843
300/BS3	24.3×10^{24}	300	1264.5	1264.5[1,2]	0.19	0.19	0	–
		450	957.7	957.7	0.79	0.15	27	−4.68
600/BS4	0.2×10^{24}	−196	2148.5	2148.5[1,2]	0.21	0.21	0	–
		−150	1798.9	1798.9	0.92	0.17	22	−0.682
		−100	1570.0	1570.0	2.28	0.05	–	−0.344
600/BS5	2.1×10^{24}	−196	1925.1	1925.1[1,2]	0.05	0.05	–	–
		−150	1854.8	1854.8	0.98	0.18	2	−0.221
		−100	1537.6	1537.6	4.53	0.13	24	−0.034
600/BS6	24.3×10^{24}	−100	1361.1	1361.1[1,2,3]	0.05	0.05	0	–
		−50	1421.1	1421.1	0.37	0.24	7	0.138

Notes:
[1] Since the uniform elongation was <0.2%, the yield strength cannot be determined, and is listed as being equal to the ultimate strength.
[2] Prompt brittle fracture was observed with a slight amount of yielding at stresses near the yield point.
[3] Initial fracture at pinhole followed by a second test shoulder loading. Results are reported for the shoulder loading test.
[4] '–' means that a value was not measured for this condition.
[5] RT = Room-temperature.

over the room-temperature DBTT observed for LSR ODS following 600 °C irradiations to higher fluences of 72.6×10^{24} n/m^2 and 246×10^{24} n/m^2. The lower DBTT of −50 °C observed at a fluence of 24.3×10^{24} n/m^2 for LAW HP-LCAC and LAW ODS may be attributed to the lower fluence as irradiation to higher fluences may produce greater irradiation hardening and elevation of the DBTT. Higher fluence irradiations above 24.3×10^{24} n/m^2 at 600 °C are needed to determine if the lower DBTT result of −50 °C observed for LAW HP-LCAC and LAW ODS Mo is maintained.

For 600 °C irradiations of LAW HP-LCAC and LAW ODS Mo to lower fluences of 2.1 and 0.2×10^{24} n/m^2, plasticity in the stress–strain curves, measurable levels of ductility (0.9–5.9% elongation and 2–25% RA), and mixed-mode failures with local ductile-laminate features were observed at temperatures of −150 °C and −100 °C. Linear-elastic stress–strain curves, no ductility, and brittle failure modes were observed at −196 °C. This indicates the DBTT for LAW HP-LCAC and LAW ODS Mo at these lower fluences is between −150 °C and −196 °C and is conservatively defined as −150 °C, which is unchanged from the non-irradiated condition.

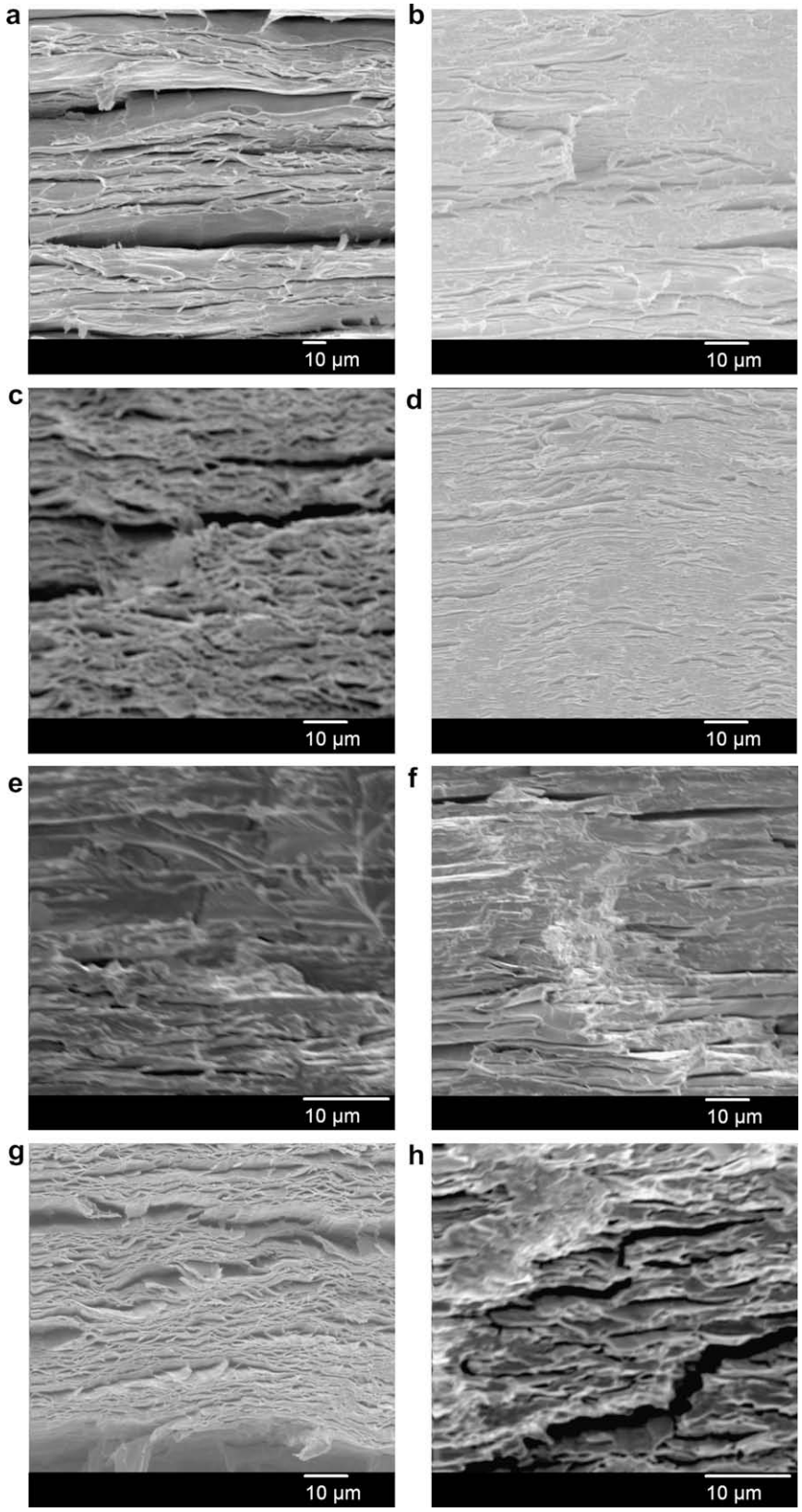

Fig. 6. Post-irradiated SEM fractography of LAW HP-LCAC Mo and LAW ODS Mo following irradiations at nominally 300 °C to fluences of 0.2, 2.1, and 24.3×10^{24} n/m^2 for tensile testing of : (a) HP-LCAC at 450 °C after irradiation to a dose of 24.3×10^{24} n/m^2 showing a ductile-laminate failure mode, (b) HP-LCAC at 300 °C after irradiation to a dose of 24.3×10^{24} n/m^2 showing a mixed-mode fracture, (c) ODS at 450 °C after irradiation to a dose of 24.3×10^{24} n/m^2 with a ductile-laminate failure mode, (d) ODS at 300 °C after irradiation to a dose of 24.3×10^{24} n/m^2 with a mixed-mode fracture, (e) HP-LCAC at −150 °C after irradiation to a dose of 2.1×10^{24} n/m^2 with a mixed-mode fracture, (f) HP-LCAC at −150 °C after irradiation to fluence of 0.2×10^{24} n/m^2 showing a mixed-mode fracture, (g) ODS at 22 °C after irradiation to a dose of 2.1×10^{24} n/m^2 with ductile-laminate, and (f) ODS at −150 °C after irradiation to 0.2×10^{24} n/m^2 showing a mixed-mode fracture.

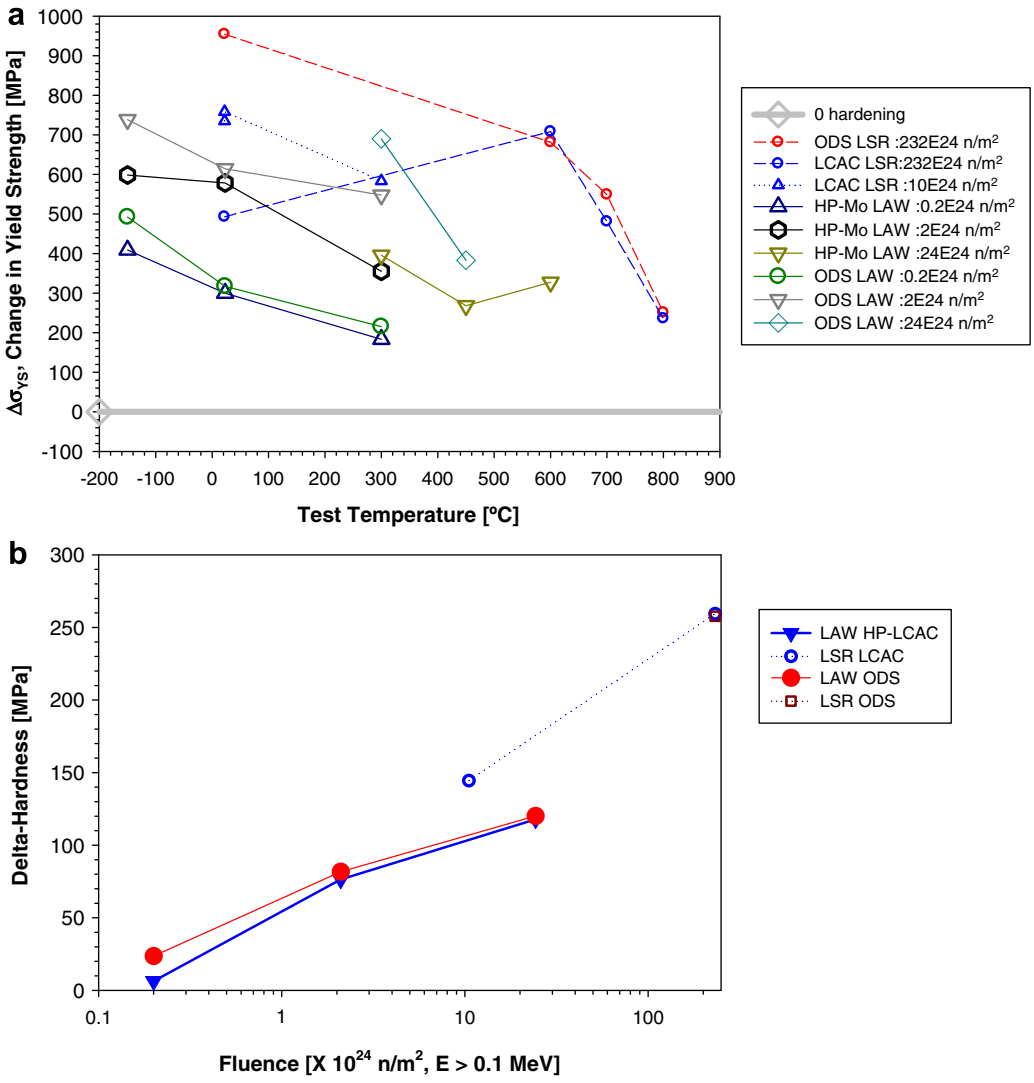

Fig. 7. Comparison of post-irradiated hardening ($\Delta\sigma_{YS} = \sigma_{YS}$ (irad) – σ_{YS} (non-irad)) determined from the tensile data and change in hardness for LAW HP-LCAC and LAW ODS irradiated at nominally 300 °C (270–309 °C) in HFIR at fluences of 0.2, 2.1, and 24.3 × 10^{24} n/m^2 ($E > 0.1$ MeV) with previously reported results for LSR LCAC and LSR ODS [27,31,32,38]: (a) post-irradiated hardening as a function of test temperature, and (b) change in hardness as a function of fluence (log-scale).

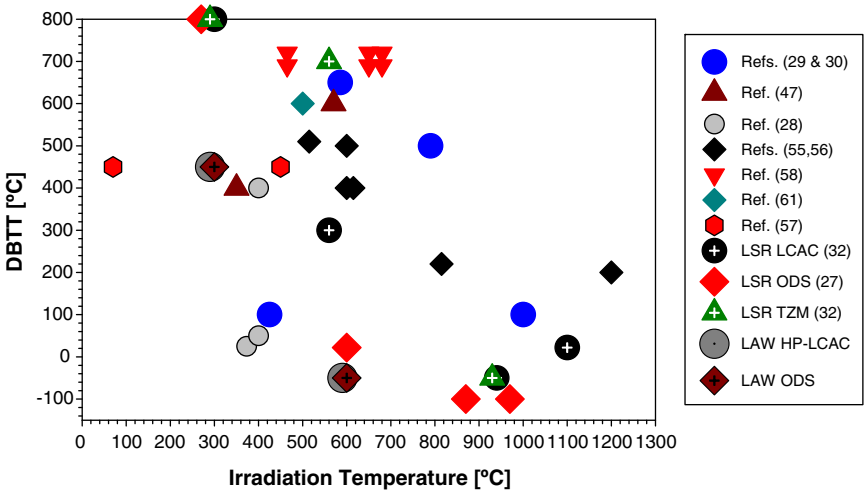

Fig. 8. Summary of results for LAW HP-LCAC and LAW ODS values for this work compared with literature data for molybdenum as a function of irradiation temperature.

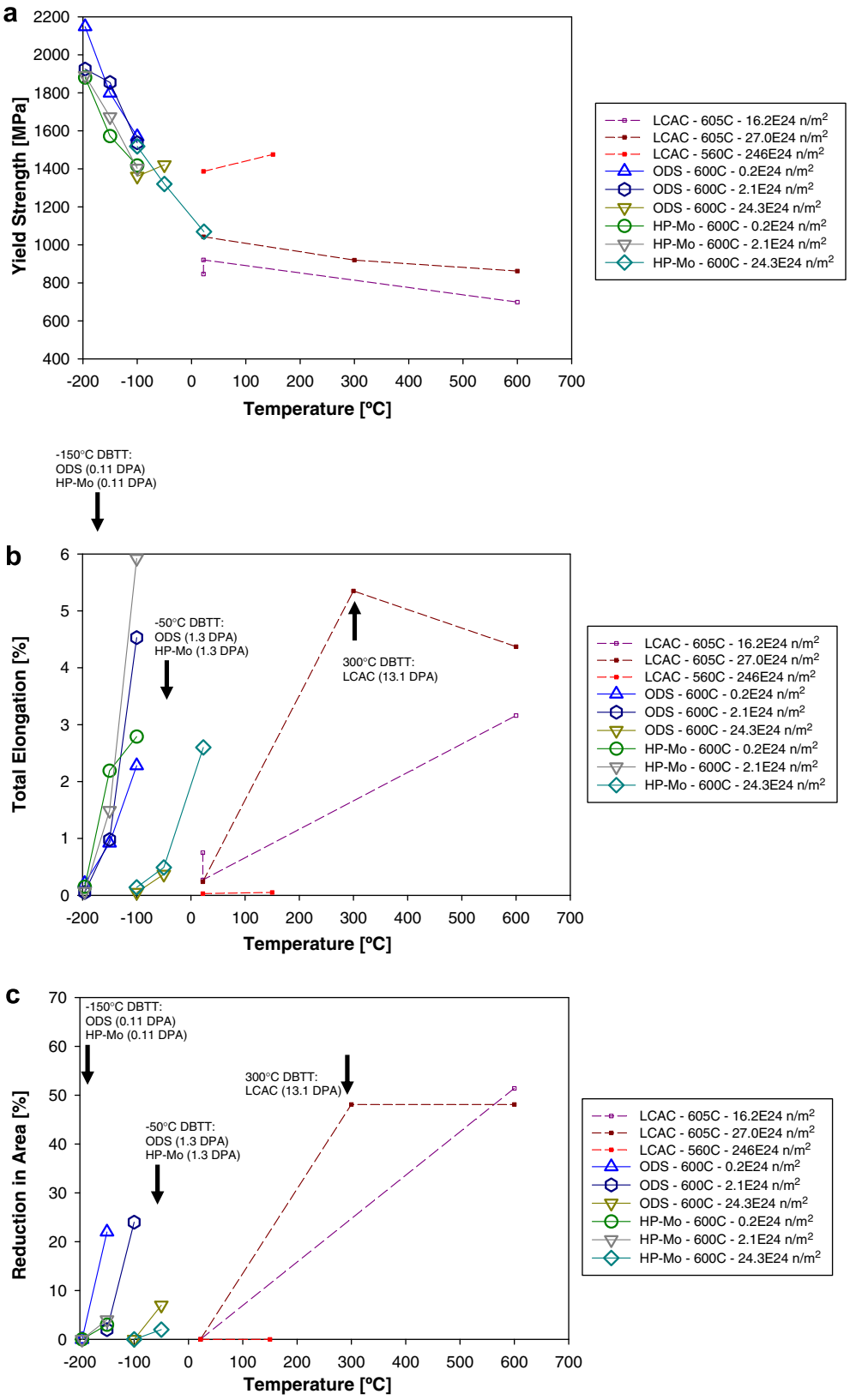

Fig. 9. Comparison of post-irradiated tensile data for LAW HP-LCAC-Mo and LAW ODS Mo sheet following irradiation in HFIR at nominally 600 °C to fluences of 0.2, 2.1, and 24.3×10^{24} n/m^2 with previously reported results for LSR LCAC [31,32]: (a) 0.2% yield strength, (b) total elongation, and (c) reduction in area. The tensile strength values determined at temperatures below the DBTT are actually a fracture stress as true plastic deformation has not been achieved.

A relatively large increase in tensile strength was observed for the 600 °C irradiations starting at the lowest fluence of 0.2×10^{24} n/m^2, but the largest increase in tensile strength and irradiation hardening was generally observed at fluences between 2.1 and 24.3×10^{24} n/m^2. The tensile strength and irradiation hardening values for LAW HP-LCAC are shown in Fig. 12 to be

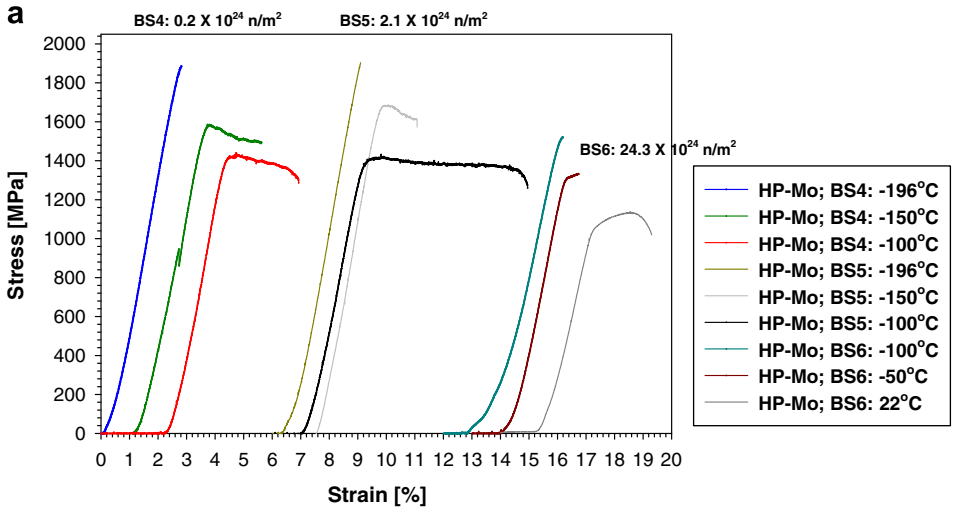

Capsule	BS4			BS5			BS6		
Test Temp	-196 °C	-150 °C	-100 °C	-196 °C	-150 °C	-100 °C	-100 C	-50 °C	22 °C
N	--	-0.110	-0.099	--	-0.110	0.009	--	0.314	0.135

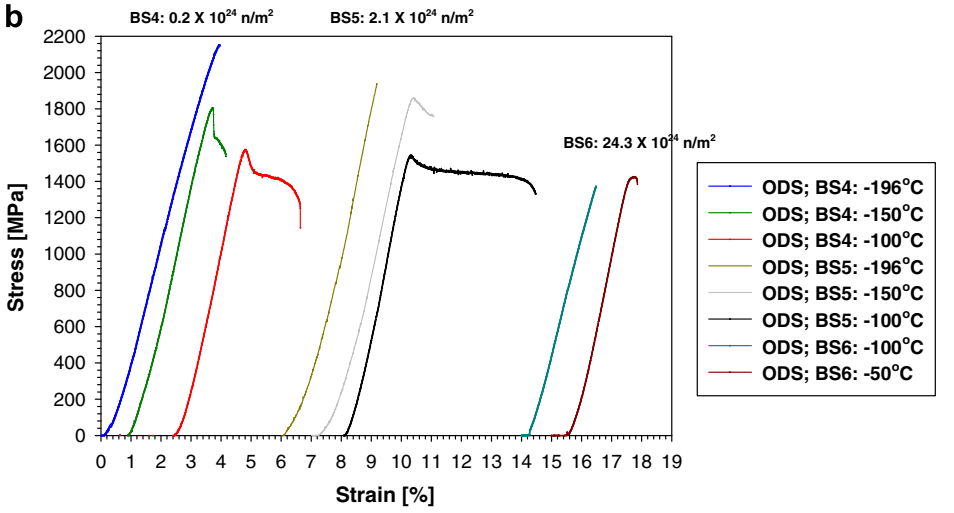

Capsule	BS4			BS5			BS6	
Test Temp	-196 °C	-150 °C	-100 °C	-196 °C	-150 °C	-100 °C	-100 °C	-50 °C
n	--	-0.682	-0.344	--	-0.221	-0.034	--	0.138

Fig. 10. Stress–strain curves for LAW High-Purity LCAC molybdenum and LAW ODS molybdenum specimens irradiated in HFIR at nominally 600 °C in capsules BS-4, BS-5, and BS-6 to nominal fluences of 0.2, 2.1, and 24.3 × 10^{24} n/m^2 (E > 0.1 MeV), respectively: (a) LAW HP-LCAC, and (b) LAW ODS. Strain hardening exponent results are also provided below and in Tables 7 and 8.

generally lower than for LAW ODS Mo at all fluences, and reported values for irradiation hardening for LSR LCAC irradiated to a slightly higher fluence of 27.0 × 10^{24} n/m^2 [31]. The lower tensile strength and irradiation hardening values for HP-LCAC Mo is indirect evidence that high-purity reduces the spacing between the hardening barriers. The tensile strength and irradiation hardening values for LAW ODS Mo were slightly higher than LAW HP-LCAC Mo over the full range of fluences and reported values for LSR LCAC irradiated to a similar fluence of 27.0 × 10^{24} n/m^2, but were lower than reported values for LSR ODS and LSR LCAC irradiated to higher fluences of 72.6–246 × 10^{24} n/m^2 [27,31,32].

The lower DBTT and lower irradiation hardening for LAW ODS Mo and LAW HP-LCAC Mo likely result from the presence of a fine grain size with fine particles and higher dislocation density (LAW ODS) and higher dislocation density and higher purity (LAW HP-LCAC-Mo). These features of the microstructure likely provide the slightly improved resistance to irradiation embrittlement for 600 °C irradiations to a maximum fluence of 24.3 × 10^{24} n/m^2. The slightly lower increase in tensile strength and irradiation hardening for LAW HP-LCAC Mo indicates that high-purity provides slightly better resistance to embrittlement for 300 °C and 600 °C irradiations to these fluences.

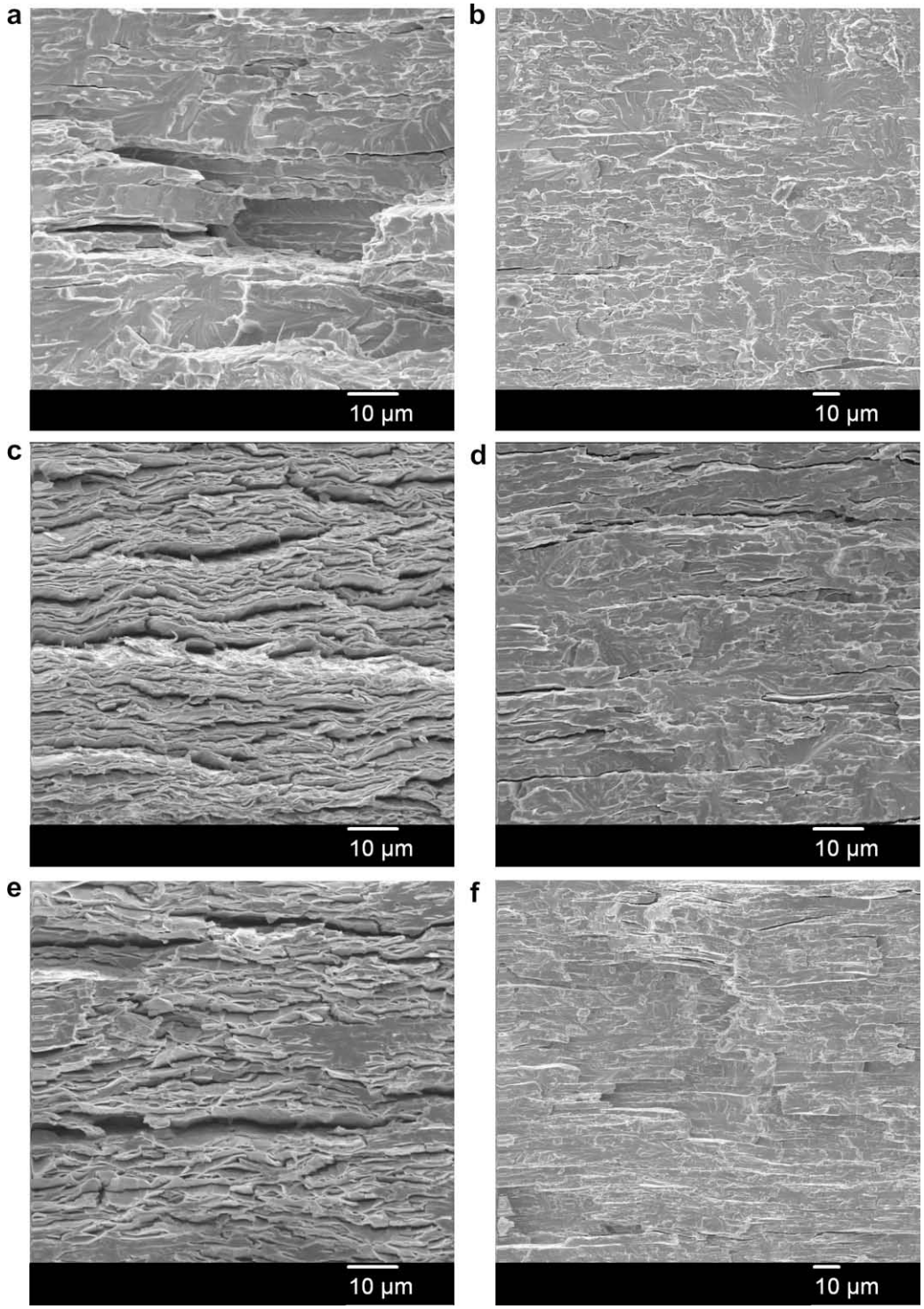

Fig. 11. Post-irradiated SEM fractography of LAW HP-LCAC Mo and LAW ODS Mo following irradiations at nominally 600 °C to fluences of 0.2, 2.1, and 24.3×10^{24} n/m^2 for tensile testing of: (a) HP-LCAC at −50 °C after irradiation to a dose of 24.3×10^{24} n/m^2 showing a mixed-mode failure, (b) HP-LCAC at −100 °C after irradiation to a dose of 24.3×10^{24} n/m^2 showing a cleavage fracture, (c) ODS at −50 °C after irradiation to a dose of 24.3×10^{24} n/m^2 with a ductile–laminate failure mode, (d) ODS at −100 °C after irradiation to a dose of 24.3×10^{24} n/m^2 with a mixed-cleavage fracture, (e) ODS at −150 °C after irradiation to a dose of 2.1×10^{24} n/m^2 with a mixed-mode fracture, (f) HP-LCAC at −150 °C after irradiation to fluence of 0.2×10^{24} n/m^2 showing a mixed-mode fracture.

3.4. Change in electrical resistivity for irradiations at nominally 300 °C and 600 °C

The change in electrical resistivity provides an indirect measurement of the increase in defect density from irradiation. The change in electrical resistivity for LAW HP-LCAC Mo is shown in Fig. 13 to be slightly less than for LAW ODS Mo for irradiations at both 300 °C and 600 °C. The slightly lower increase in electrical resistivity for HP-LCAC is indirect evidence that higher purity results in a reduced number density of the hardening centers that produce scattering. This is in agreement with tensile results where the slightly lower irradiation hardening observed for HP-LCAC also indicates an increase in the spacing between defects.

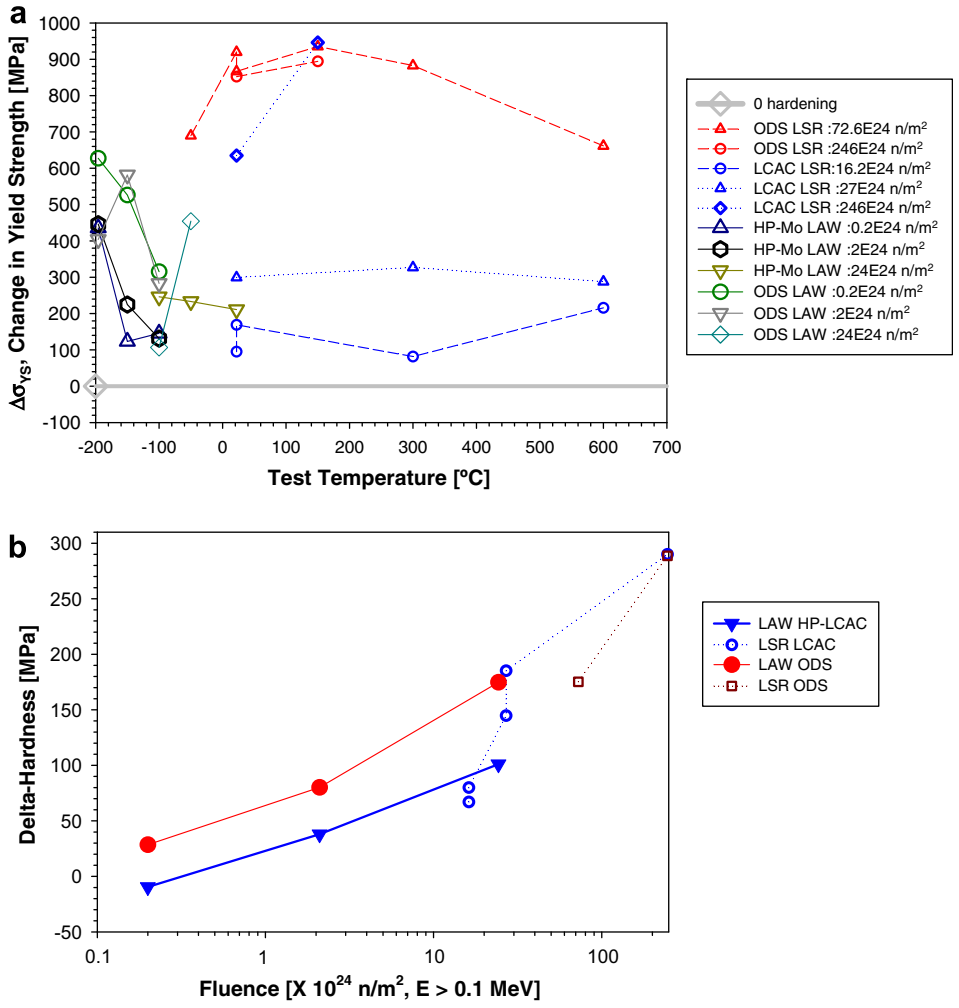

Fig. 12. Post-irradiated hardening ($\Delta\sigma_{YS} = \sigma_{YS}$ (irad) $- \sigma_{YS}$ (non-irad)) determined from the tensile data and change in hardness for LAW HP-LCAC and LAW ODS irradiated at nominally 600 °C (560–605 °C) in HFIR at fluences of 0.2, 2.1, and 24.3 $\times$ 10^{24} n/m^2 ($E > 0.1$ MeV) compared with reported results for LSR LCAC and LSR ODS [27,31,32,38]: (a) post-irradiated hardening as a function of test temperature, and (b) change in hardness as a function of fluence (log-scale).

Larger changes in electrical resistivity were observed for the 300 °C irradiations in comparison to the 600 °C irradiations which is attributed to a higher number density of defects. The largest change in electrical resistivity for the 300 °C irradiation occurs at lower fluences of 0.2 $\times$ 10^{24} n/m^2, while the larger changes in electrical resistivity for the 600 °C irradiations occur between fluences of 2.1 and 24.3 $\times$ 10^{24} n/m^2. Slower point defect mobility for the 300 °C irradiations results in the formation of a higher number density of voids/loops at lower fluence than for the 600 °C irradiations. The increase in electrical resistivity as a function of fluence is shown in Fig. 13 to be sub-linear with dose.

3.5. TEM examinations of microstructure for irradiations at nominally 300 °C and 600 °C

Representative TEM micrographs for HP-LCAC Mo and ODS Mo irradiated at 300 °C and 600 °C are shown in Figs. 14–17. A summary of average void/loop size and number density values determined from TEM examinations of microstructure and calculated and measured values of irradiation hardening for the 300 °C and 600 °C irradiations are shown in Table 9. Void hardening is calculated using the Orowan equation where G is the shear modulus, b is the Burgers vector, l_v is the spacing between voids, d_v is the void diameter, N_v is the number density of voids, and $\alpha(i)$ is a strength barrier term unique to each equation such that $0 < \alpha_{(i)} \leqslant 1$ [62–65]:

$$\sigma_{OR} = \alpha_{(1)}(2Gb)/l_v = 2\alpha Gb(d_v N_v)^{1/2}. \quad (1)$$

Assuming void cutting occurs or the voids are 'soft barriers', a second equation provides a lower bound for void hardening [62]:

$$\sigma_{SV} = \alpha_{(2)}(Gb(d_v N_v)^{1/2})(\ln(R_v/r_d)/2\pi), \quad (2)$$

where R_v is the radius of the void and r_d is the radius of the dislocation core. Loop hardening is described by the following equation [62,63]:

$$\sigma_{ORL} = [\alpha_{(3)}(Gb)/2](d_{loop}N_{loop})^{1/2}. \quad (3)$$

Faceted voids have been observed for molybdenum irradiated to 600 °C and 900 °C [44,53–61,63,64]. However, clear evidence for facets has not been observed for the 300 °C irradiations that may suggest the cavities are voids. Although this work does not prove the observed cavities are indeed voids, all cavities observed in this work are described as voids herein to be consistent with the literature for irradiated molybdenum. Average values for void and loop size and number density were used in the calculations. Since the void and loop distributions were very narrow and generally symmetric or normal, calculations made using a summation of

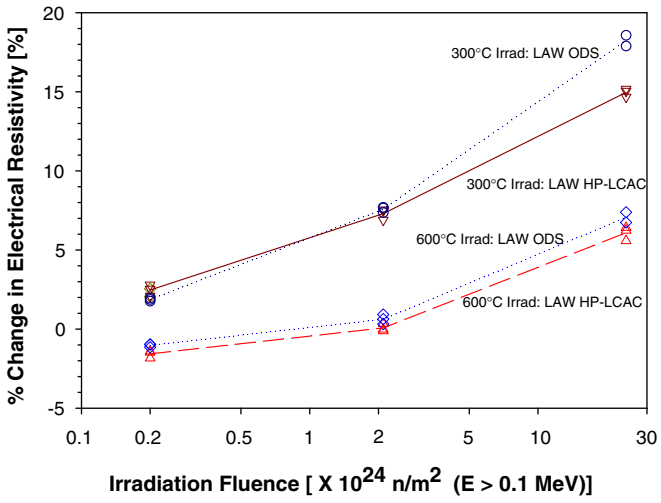

Fig. 13. Summary of the percentage change in electrical resistivity determined from pre- and post-irradiated electrical resistivity measurements made at room-temperature following the irradiation of LAW HP-LCAC and LAW ODS at nominally 300 °C and 600 °C to fluences of nominally 0.2, 2.1, and 24.3×10^{24} n/m^2 ($E > 0.1$ MeV). The lines connect the average values and fluence is on a log scale.

the distribution were comparable to results determined using the average values.

For the 300 °C irradiations, Figs. 14 and 15 show that a high number density of dislocation loops and voids were observed, but the loops are much larger in size and are much lower in number density than the voids, see Table 9. Although reported in the literature, no ordering of voids was resolved. The loop sizes for LAW HP-LCAC Mo were slightly larger than values for LAW ODS Mo, while a slightly larger loop number density was observed for LAW ODS. These results indicate that differences in purity and grain size have little effect on the size and number density of loops for 300 °C irradiations. Voids are shown in Table 9 to have a much higher number density and are much stronger hardening barriers than loops with a factor of 22.3–4.7 larger void hardening calculated. Thus, voids have a dominant effect on hardening for the 300 °C irradiations. Insensitivity of the developing defect population to pre-existing microstructure suggests that point defect concentrations are controlled by mutual recombination in this environment rather than absorption at sinks.

For the 300 °C irradiations, the void sizes for LAW HP-LCAC Mo were slightly larger than LAW ODS Mo at the higher fluences, while the void number densities for LAW HP-LCAC were lower than LAW ODS with a larger difference observed at the higher fluence of 24.3×10^{24} n/m^2. A general increase in void size and number den-

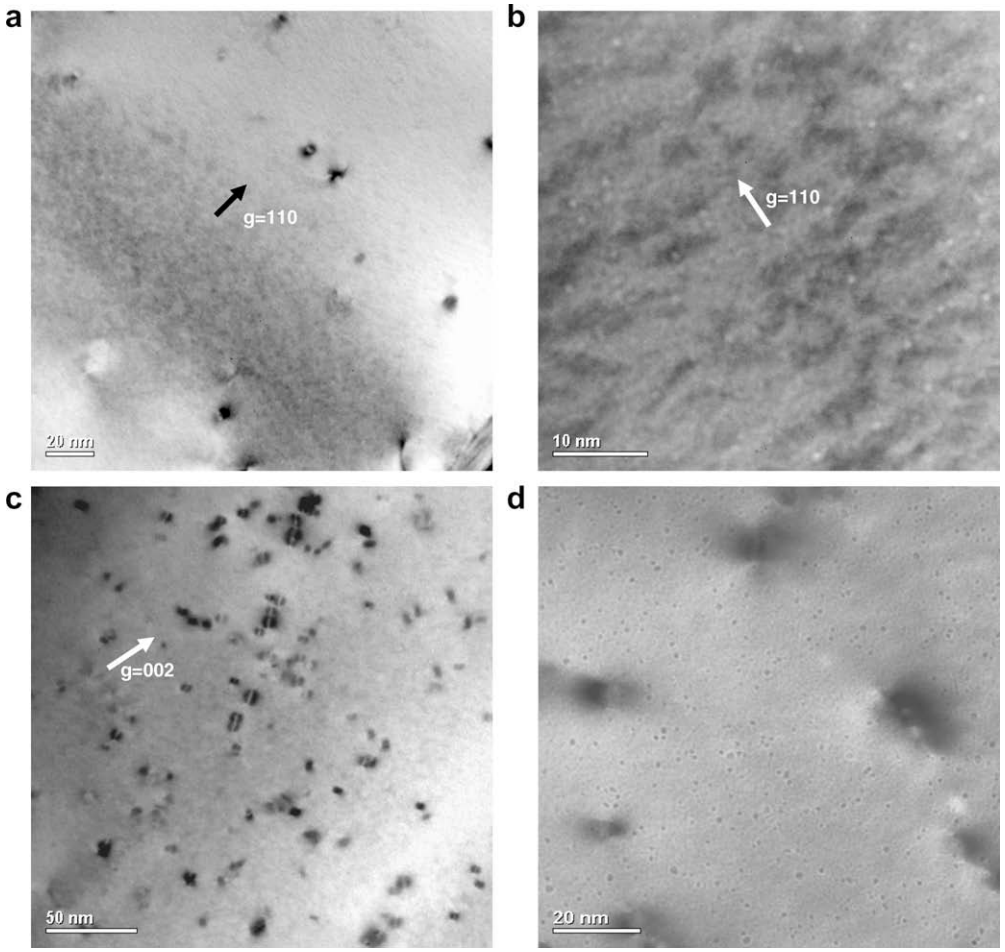

Fig. 14. Representative TEM images of cavities (also known as voids) and loops observed from post-irradiated examinations of LAW HP-LCAC following HFIR irradiations at nominally 300 °C to fluences of 0.2, 2.1, and 24.3×10^{24} n/m^2 ($E > 0.1$ MeV): (a) image of loops for irradiation to a fluence of 0.2×10^{24} n/m^2, (b) image of cavities for irradiation to a dose of 0.2×10^{24} n/m^2, under-focus, (c) micrograph of loops from irradiation to a fluence of 2.1×10^{24} n/m^2, (d) image of cavities for irradiation to a dose of 2.1×10^{24} n/m^2, over-focus, (e) micrograph of loops for irradiation to a dose of 24.3×10^{24} n/m^2, (f) images of cavities for irradiation to a dose of 24.3×10^{24} n/m^2, over-focus, and (g) and (h) images from irradiation to a fluence of 24.3×10^{24} n/m^2 near a grain boundary, under-focus.

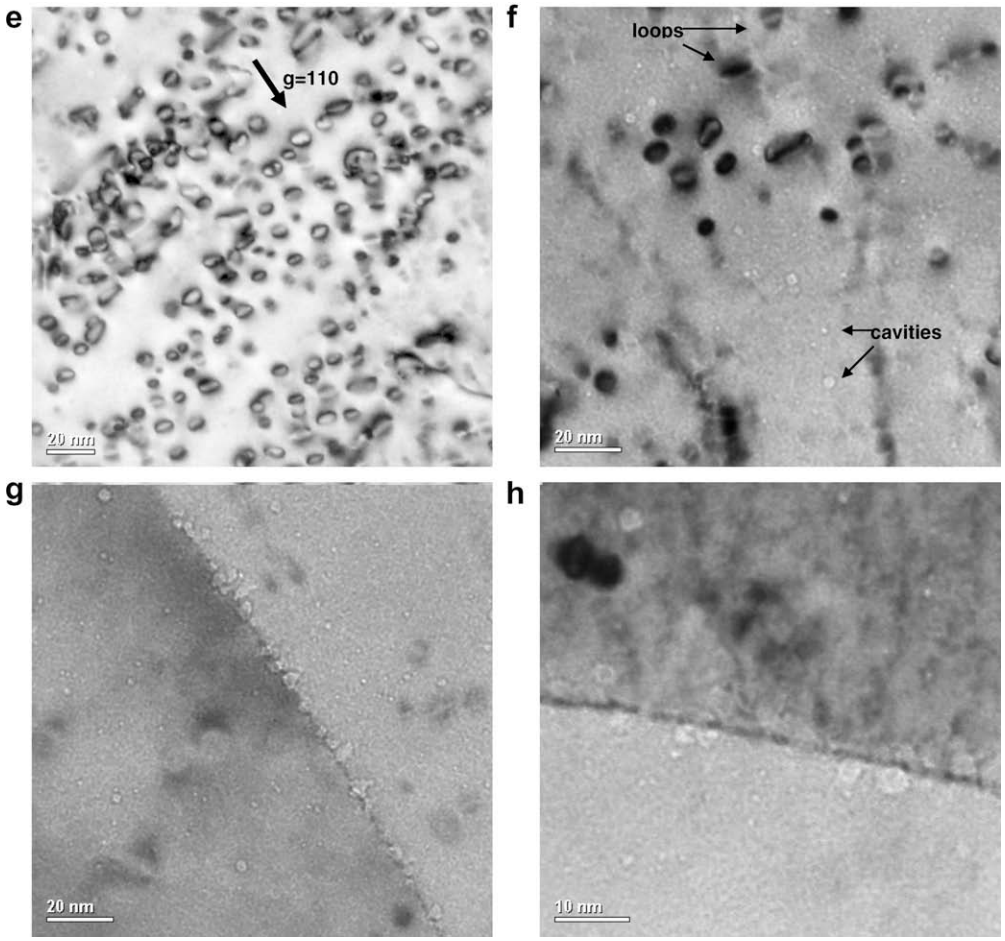

Fig. 14 (*continued*)

sity is observed for LAW ODS Mo at higher fluences. Although LAW HP-LCAC Mo exhibits a void size increase with fluence, the number density actually decreases between 2.1×10^{24} n/m^2 and 24.3×10^{24} n/m^2. At the highest fluence of 24.3×10^{24} n/m^2 the lower void number density values for LAW HP-LCAC Mo results in lower calculated void hardening values that are consistent with the slightly lower measured irradiation hardening for LAW HP-LCAC at this dose. Grain boundaries and network dislocations are sinks for point defects, and the higher density of these sites present in LAW ODS and LAW HP-LCAC Mo may suppress the nucleation of voids and result in the slightly lower irradiation hardening and slightly lower DBTT compared to LSR LCAC [31]. Higher residual stresses from the high dislocation density for the LAW condition may also contribute to improved resistance to irradiation embrittlement. However, the high dislocation density does not appear to be maintained at higher fluences, suggesting the benefit of increased dislocation density on reducing the concentration of point defects would not be maintained at higher neutron fluences.

For the 300 °C irradiations, the lowest void number density, lower calculated and measured irradiation hardening, lower DBTT at a fluence of 2.1×10^{24} n/m^2, and lower change in electrical resistivity was observed for LAW HP-LCAC Mo. This indicates that higher purity levels may allow for faster movement of point defects to pre-existing sinks, especially neutral grain boundaries, that results in a lower void number density, slightly less irradiation hardening and slight improvements in properties over the fluence range evaluated ($0.2–24.3 \times 10^{24}$ n/m^2).

For the 600 °C irradiations, Figs. 16 and 17 show that a low number density of relatively large loops and higher number density of voids were observed for LAW ODS Mo and LAW HP-LCAC Mo at the lowest fluence of 0.2×10^{24} n/m^2. Only relatively high number density of voids are observed for LAW ODS and LAW HP-LCAC-Mo at the highest fluence of 24.3×10^{24} n/m^2. Dislocation loops have been observed in TEM examinations of molybdenum and molybdenum alloys irradiated at temperatures near 600 °C to low fluences, but are not observed or have a very low number density and large size for 600 °C irradiations to higher fluence [4,28,30,44,61,63,64,66–72]. This suggests that low number densities of loops may form in molybdenum during 600 °C at low fluences, but evolution of the microstructure so that voids are prominent occurs at higher fluences. Although reported in the literature, the ordering of voids was not observed.

For the 600 °C irradiations, an increase in the size and number density of voids is observed at higher fluences for LAW HP-LCAC and LAW ODS Mo. The void sizes for LAW HP-LCAC Mo are lower than LAW ODS at the highest fluence (24.3×10^{24} n/m^2), but both have a similar void number density. The lower void diameter results in slightly lower calculated void hardening for HP-LCAC Mo that is consistent with the slightly lower measured irradiation hardening and change in electrical resistivity for LAW HP-LCAC in comparison to LAW ODS Mo. This indicates that increased purity likely results in faster movement of point defects to both biased and non-biased sinks at more comparable rates so that the void population is reduced to result in a slightly better mitigation of irradiation embrittlement for irradiations at both 300 °C and 600 °C. Although reported in the literature for higher dose irradiations, no ordering of the voids was observed for the 600 °C irradiations.

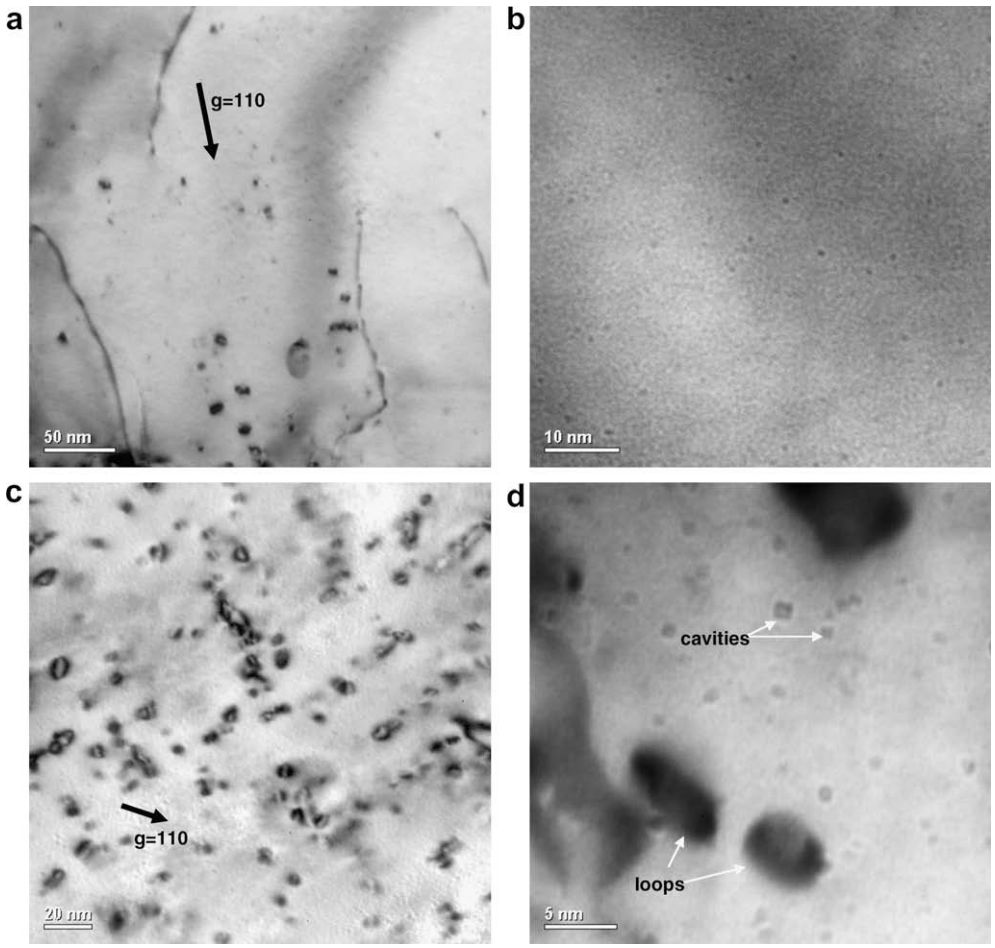

Fig. 15. Representative TEM images of cavities (also known as voids) and loops observed from post-irradiated examinations of LAW ODS Mo following HFIR irradiations at nominally 300 °C to fluences of 0.2 and 24.3 $\times$ 10^{24} n/m^2 (E > 0.1 MeV): (a) image of loops from a specimen irradiated to a fluence of 0.2 $\times$ 10^{24} n/m^2, (b) image of cavities for irradiation to a dose of 0.2 $\times$ 10^{24} n/m^2, over-focus, (c) micrograph of loops from a specimen irradiated to a dose of 24.3 $\times$ 10^{24} n/m^2, (d) images of cavities after irradiation to a dose of 24.3 $\times$ 10^{24} n/m^2, over-focus.

Although the measured irradiation hardening for 600 °C irradiated LAW HP-LCAC and LAW ODS Mo are similar to that observed for LSR LCAC, a significantly lower DBTT of −50 °C was observed for LAW HP-LCAC and LAW ODS than the 300 °C value exhibited by LSR LCAC [31,32]. Relatively wide void-denuded zones that are nominally 25–20 nm in width on each side of the grain boundary are observed for HP-LCAC and LAW ODS Mo (Figs. 16(d) and 17(d)). Grain boundaries and particle interfaces are generally considered neutral sinks for the point defects produced by irradiation, and void-denuded zones are observed near grain boundaries and particle interfaces. The low mobility for point defects results in void-denuded zones that are negligible in width for the 300 °C irradiations (Figs. 14(g) and(h)). Void coarsening is observed at grain boundaries for 300 °C irradiated LAW HP-LCAC Mo and LAW ODS Mo that does not enhance the ductile-laminate failure mechanism.

The finer grain size and oxide particles present in LSR ODS [27] and LAW ODS and LAW HP-LCAC Mo results in a higher concentration of void-denuded zones and defect-free regions for the 600 °C irradiations. This appears to improve the fracture resistance of the material near the boundaries and results in a significantly lower DBTT for LSR and LAW ODS and HP-LCAC-Mo irradiated at 600 °C, see Fig. 8. The denuded zones observed at interfaces likely lead to the formation of small ductile ligaments during fracture by the ductile-laminate toughening mechanism that result in improved toughening and a lower DBTT [27]. Finer grains also limit the length of dislocation pile-ups that can lead to crack nucleation and can disrupt the length over which dislocation channels can develop. The low DBTT for LAW ODS and LAW HP-LCAC Mo following the 600 °C irradiations may result from the finer grain size, higher dislocation density, and higher purity.

Irradiation at 300 °C results in the formation of a higher number density of small voids/loops than produced for the 600 °C irradiations. The closer void spacing for the 300 °C irradiations results in slightly larger irradiation hardening, increase in DBTT, and change in electrical resistivity for LAW HP-LCAC and LAW ODS Mo compared to the 600 °C irradiations. The slower mobility of point defects, and the inherent disparity in mobility and bias of sinks removes interstitials to leave a higher concentration of vacancies, results in a higher super saturation of vacancies and therefore the formation of this higher number density of voids at much lower fluences for the 300 °C irradiations, and produces a much larger increase in hardening and electrical resistivity at lower fluences of 0.2–2.1 $\times$ 10^{24} n/m^2 for the 300 °C irradiations. Larger increases are generally delayed until fluences of 24.3 $\times$ 10^{24} n/m^2 for the 600 °C irradiations. The relatively large void number density and larger void size for 600 °C irradiated LAW HP-LCAC-Mo and LAW ODS results in relatively high hardening. However, the DBTT for LAW HP-LCAC and LAW ODS Mo irradiated at 600 °C (−50 °C) is much lower than observed for the 300 °C irradiations (450 °C). The formation of the wider void-denuded zone for the 600 °C irradiations that are thought to result in improved ductile-laminate toughening for fine grained materials such as

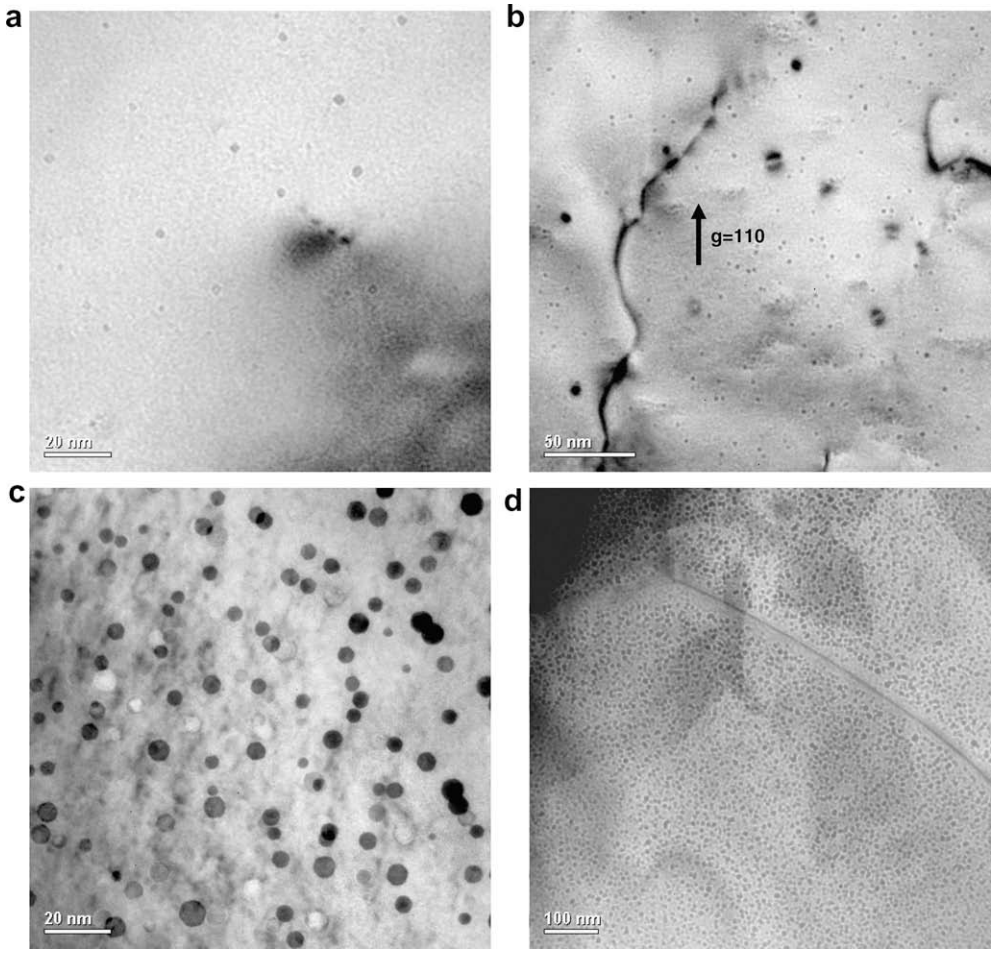

Fig. 16. Representative TEM images of cavities (also known as voids) and loops observed from post-irradiated examinations of LAW HP-LCAC Mo following HFIR irradiations at nominally 600 °C to fluences of 0.2 and 24.3 × 10^{24} n/m^2 (E > 0.1 MeV): (a) image of cavities from a specimen irradiated to a fluence of 0.2 × 10^{24} n/m^2, over-focus, (b) image of loops for irradiation to a dose of 0.2 × 10^{24} n/m^2, over-focus, (c) micrograph of cavities from a specimen irradiated to a dose of 24.3 × 10^{24} n/m^2, over-focus, and (d) images of denuded zone near grain boundary for cavities from irradiation to a dose of 24.3 × 10^{24} n/m^2, over-focus.

LAW HP-LCAC-Mo and LAW ODS is likely the reason for the lower DBTT for the 600 °C irradiations.

Calculated irradiation hardening values from TEM examinations Eq. (1) for all molybdenum alloys and materials are a factor of 1.8–8.8 larger than the measured irradiation hardening for irradiations at 300 °C, and a factor of 2.7–11.5 higher for 600 °C irradiations. Void cutting could explain the difference between calculated and measured hardening, but mechanistic modeling and microstructure examinations of deformed material are needed to confirm this mechanism. Void ordering that could also explain such a difference in calculate/measured hardening was also not observed. The lower interstitial content for HP-LCAC Mo, fine grain size, and high dislocation density may also serve to reduce the void barrier strength term (α) because the concentration of interstitials (oxygen or carbon) that may harden voids is lower. It must also be recognized that for any samples tested below the DBTT, only a lower bound on the increase in yield strength can be established since the material fractures before yielding. The large difference between calculated and measured irradiation hardening can be explained in part by the fact that the tensile strength measured at temperatures below the DBTT is a fracture stress and irradiation hardening is not truly being measured. Irradiation embrittlement results from elevation of the flow stress above the fracture stress so that brittle fracture occurs from pre-existing flaws. The calculated irradiation hardening values may be representative of the flow stress.

The lower void number density for LAW HP-LCAC Mo for the 300 °C irradiations, lower void size, lower measured hardening, lower calculated irradiation hardening, lower DBTT values at lower fluences, and lower change in electrical resistivity, are relatively small differences compared to LAW ODS Mo and previously reported results for LSR LCAC Mo [31,32] that indicate higher purity can provide a small improvement in mitigation of irradiation embrittlement for molybdenum materials that have a fine grain size on the order of 1 μm and a high dislocation density in the fluence range of 0.2–24.3 × 10^{20} n/m^2. The lower DBTT for LAW ODS compared to LSR LCAC and literature data (Fig. 8) indicates that a fine grain size, fine particle size, and increased dislocation density can also lead to a slight improvement in resistance to irradiation embrittlement.

3.6. Irradiation defect formation by nucleation and growth

An increase in irradiation hardening, tensile strength, DBTT, percent change in electrical resistivity, and void size/number density is generally observed to increase at low fluences between 0.2 and 24.3 × 10^{24} n/m^2 (0.011–1.29 dpa) with a sub-linear fluence dependence ($(\phi t)^n$ dependence where $n < 1$) for the irradiations of LAW HP-LCAC Mo and LAW ODS Mo at nominally 300 °C and 600 °C. The increase in defect size and number density correlates with the increase in properties that are directly proportional to defect spacing such as tensile strength and electrical resistivity in this

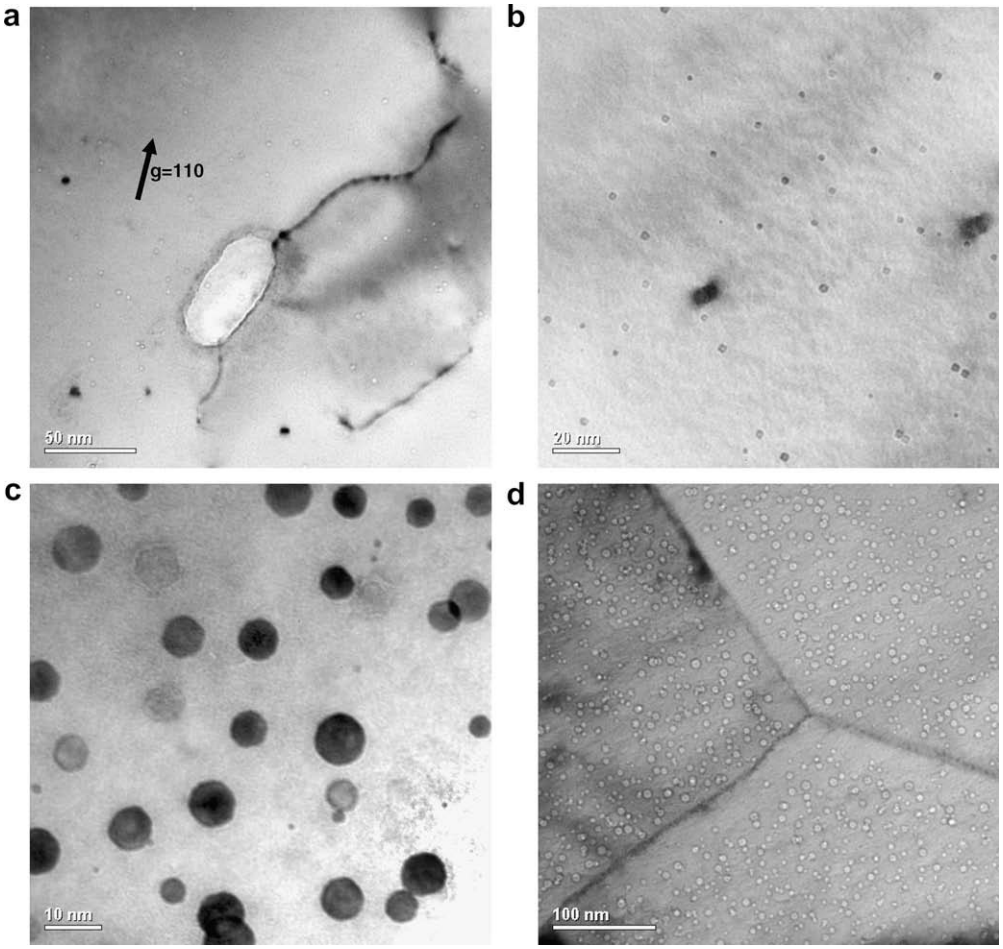

Fig. 17. Representative TEM images of cavities (also known as voids) and loops observed from post-irradiated examinations of LAW ODS Mo following HFIR irradiations at nominally 600 °C to fluences of 0.2 and 24.3 × 10^{24} n/m^2 (E > 0.1 MeV): (a) image of cavities from a specimen irradiated to a fluence of 0.2 × 10^{24} n/m^2, under-focus, (b) image of loops for irradiation to a dose of 0.2 × 10^{24} n/m^2, over-focus, (c) micrograph of cavities from a specimen irradiated to a dose of 24.3 × 10^{24} n/m^2, over-focus, and (d) image of a denuded zone near grain boundary for cavities after irradiation to a dose of 24.3 × 10^{24} n/m^2, under-focus.

low fluence range, and indicates that the formation of the extended defects that produce irradiation hardening and embrittlement (voids and loops) occurs by a nucleation and growth process. This conclusion is supported by the MD simulations described below.

Extended sessile point defect clusters are not formed in the displacement cascade. The formation of sessile defect clusters in the displacement cascade would be expected to result in a linear fluence dependence for the number density of defects, irradiation hardening, and change in electrical resistivity followed by saturation at relatively low fluences generally less than 1 dpa [33–36,73]. This indicates that modification of the microstructure and/or chemistry of molybdenum can be used to influence point defect transport behavior and, therefore, decrease the size and number density of extended defect clusters (voids/loops) to mitigate irradiation embrittlement.

3.7. Molecular dynamics simulations

In order to gain additional insight into the mechanism by which hardening defects form in molybdenum, molecular dynamics simulations were run at Bettis for a large number of displacement cascades to determine the geometrical configuration of point defects remaining after the initial formation and collapse of the cascade roughly 8 ps following the PKA. The calculations were done to assess whether or not there was a tendency to form large extended defects directly from the cascades.

Clustering behavior can be quantified by computing a distribution function expressing the number of defects that exist within clusters of varying size. Defects that lie within one nearest neighbor distance of one another are considered to belong to the same cluster. Cluster analysis can be most easily performed using a linked list, depth first search methodology described previously [74]. The analysis has been performed for both the stable interstitial and vacancy populations of each of the MD simulations. The results are tabulated in Tables 10 and 11. From the tables it is clear that there is no tendency for larger, multi-defect clusters to form directly from the kinetics of the cascade event itself. While the small defect clusters may form the nuclei of larger defects that are significant obstacles to dislocation flow, it is clear that some degree of atomic diffusion will be necessary for their growth.

4. Summary

HFIR irradiations of LAW HP-LCAC Mo and LAW ODS Mo were performed at nominally 300 °C and 600 °C to fluences of 0.2, 2.1, and 24.3 × 10^{20} n/m^2 (E > 0.1 MeV). The results of tensile testing, fractography, electrical resistivity measurements, hardness measurements, and TEM examinations of microstructure are used to understand and evaluate the effect of grain size, fine particles, dislocation density, and purity on irradiation embrittlement. The increase in the size and number density of voids/loops, irradiation

Table 9
Summary of average void/loop diameter and number density values, measured and calculated irradiation hardening, change in DBTT, and % change in electrical resistivity for irradiations of LAW HP-LCAC and LAW ODS Mo at nominally 300 °C and 600 °C Previously reported results for LSR ODS and LSR LCAC are also shown [27,31,32]

Alloy	Fluence [x10^{24} n/m^2, E > 0.1 MeV]	[4]Void diameter (nm)	Void number density (#/cm^3)	[4]Loop diameter (nm)	Loop number density (#/cm^3)	Calc Orowan $\Delta\sigma$, voids, Eq. (1) (MPa)	Calc $\Delta\sigma$, void cutting, Eq. (2) (MPa)	Calc Orowan $\Delta\sigma$, loops, Eq. (3) (MPa)	[5]Meas. $\Delta\sigma$ at T < DBTT, (MPa)	Meas. ΔDBTT, (°C)	Average % change in electrical resistance (%)
300 °C Irradiations											
LAW HP-LCAC-Mo	0.2	0.6 ± 0.3/0.4–0.9	3.2×10^{17}	2.7 ± 1.2/0.9–6.6	2.5×10^{15}	938	−22.1	44.1	409–183	0	2.5
	2.1	0.8 ± 0.4/0.4–2.1	1.6×10^{18}	4.1 ± 2.1/0.6–15.6	1.0×10^{16}	2420	−29.6	108.3	598–355	0	7.3
	24.3	1.3 ± 0.8/0.4–5.4	8.8×10^{16}	3.9 ± 1.7/0.9–12.0	2.1×10^{16}	724	4.8	153.1	396–268	600	15.0
LAW ODS	0.2	0.6 ± 0.1/0.4–1.0	4.5×10^{17}	3.8/1.9–5.3	1.2×10^{16}	1110	−26.2	114.5	492–216	0	1.9
	24.3	0.9 ± 0.4/0.4–1.4	5.1×10^{17}	2.8 ± 1.2/0.9–7.4	2.6×10^{16}	1448	−11.0	144.1	690–383	600	18.2
LSR LCAC	10.5	[1]N/A	N/A	N/A	N/A	N/A	N/A	N/A	758–461	700	10.1
	232	[1]N/A	N/A	N/A	N/A	N/A	N/A	N/A	703–481	900	N/A
LSR ODS	232	[1]N/A	N/A	N/A	N/A	N/A	N/A	N/A	952–549	900	N/A
600 °C Irradiations											
LAW HP-LCAC-Mo	0.2	2.3 ± 0.9/0.4–5.5	2.4×10^{16}	4.9 ± 2.2/1.7–10.3[2]–	6.5×10^{14}	502	15.2	25.5	436–123	0	−1.6
	24.3	4.7 ± 1.7/0.9–11.3	5.6×10^{16}		–	1096	63.4	–	246–211	100	6.1
LAW ODS	0.2	2.0 ± 0.8/0.4–4.5	3.1×10^{16}	[3]2.4–7.2[2]–	$<5 \times 10^{14}$	532	13.1	26.2	627–316	0	−1.0
	24.3	5.8 ± 2.0/0.6–11.9	5.7×10^{16}		–	1227	81.4	–	454–107	100	7.1
LSR LCAC	16.2	[1]N/A	N/A	N/A	N/A	N/A	N/A	N/A	169–95.2	100–400	2.4
	27.0	[1]N/A	N/A	N/A	N/A	N/A	N/A	N/A	327–285	400	4.1
	246	[1]N/A	N/A	N/A	N/A	N/A	N/A	N/A	945–635	400	N/A
LSR ODS	72.6	[1]N/A	N/A	N/A	N/A	N/A	N/A	N/A	917–690	123	N/A
	246	[1]N/A	N/A	N/A	N/A	N/A	N/A	N/A	855	123	N/A

Notes:
[1] NA means that data are not available.
[2] Dislocation loops were not observed.
[3] The number density of loops was too low to gather a meaningful average diameter. Instead, a range of loop diameters is given.
[4] The average value, standard deviation and range are given for the loop and cavity size diameters. In cases where the number density of loops/voids is very low or uncertain (in the case of voids where small sizes are observed), only a range and/or average value are given.
[5] Measured $\Delta\sigma$ was determined at test temperatures below the DBTT where a brittle failure mode was observed. These are lower bound measurements of irradiation hardening.
[6] The calculated values for void and loop hardening represent a hardening barrier term of $\alpha = 1.0$.

Table 10
Average number of clusters of size 1–10 determined from MD simulations

T/*E* (KeV)	Vacancies									
	1	2	3	4	5	6	7	8	9	10+
298 K										
1	2.6									
2	5.8	0.2								
5	12.2	0.6								
10	14.6	0.4	0.6							
20	35.6	1.2								
40	65.8	1.4	0.2							
573 K										
1	2.6									
2	5.4									
5	10.6	0.4								
10	14.6	0.6				0.2				
20	36.0	0.4	0.2							
40	57.2	1.6	0.4	0.2						
923 K										
1	3.8	0.2								
2	6.0									
5	7.4	0.6								
10	15.0	0.4								
20	31.4	0.4		0.2						
40	61.3	1.8	0.5							

Table 11
Average number of clusters of size 1–10 determined from MD simulations

T/*E* (keV)	Interstitials									
	1	2	3	4	5	6	7	8	9	10+
298 K										
1	2.6									
2	5.0	0.6								
5	8.6	1.4	0.4	0.2						
10	12.8	1.6	0.4							
20	27.2	2.6	1.0	0.8	0.2					
40	48.0	7.0	1.4	0.4	0.2					
573 K										
1	2.6									
2	5.4									
5	8.0	0.8		0.2	0.2					
10	10.4	1.6	0.8		0.2					
20	25.8	3.0	1.2		0.4					
40	40.6	4.6	1.4	0.6	0.8					
923 K										
1	3.6		0.2							
2	6.0									
5	7.8	0.4								
10	10.2	2.0	0.4							
20	23.2	2.8	1.0	0.2						
40	47.0	4.3	0.8	0.5						

hardening and electrical resistivity in this low dose range (0.011–1.3 dpa) follows a sub-linear fluence dependence indicating the formation of the extended defects that produce irradiation hardening in molybdenum result from a nucleation and growth process rather than the formation of sessile defects in the displacement damage cascade. The formation of sessile defect clusters in the displacement cascade would be expected to result in a linear fluence dependence for the number density of defects followed by saturation at low fluences generally less than 1 dpa. This conclusion is supported by molecular dynamics (MD) simulations of cascade damage which does not reveal large clusters forming directly in the cascade. This suggests that modification of microstructure can be used to reduce the size and number density of defects that produce irradiation hardening and embrittlement in molybdenum.

The fine grain size and increased initial dislocation density for LAW HP-LCAC and LAW ODS Mo result in slightly lower irradiation hardening and lower DBTT values (450 °C) following 300 °C irradiations in comparison to reported results for LSR LCAC (DBTT = 600 °C) irradiated to a lower dose [31,32]. The closer spacing of pre-existing sinks (grain boundaries and dislocations) for LAW HP-LCAC and LAW ODS Mo likely produces a slight decrease in size and number density of voids so that slightly lower irradiation hardening and DBTT values are produced for the 300 °C irradiations.

The higher number density of voids/loops produced by the 300 °C irradiations, as compared to irradiation at 600 °C, results in higher irradiation hardening, increase in DBTT, and electrical resistivity values than for the 600 °C irradiations of LAW HP-LCAC and LAW ODS Mo. Although the overall density of voids in the 600 °C irradiation is comparable (between 1/3 and ½) to that seen at 300 °C, a pronounced denuded zone exists near grain boundaries at 600 °C that is not observed for 300 °C irradiations. As a result, overall hardness and yield stress, that are controlled by microstructural impediments to dislocation flow, are similar at each temperature, but the DBTT, the minimum test temperature at which some ductility is observed, is substantially lower in the samples irradiated at 600 °C (DBTT = −50 °C), due to the ability of localized flow near the grain boundaries to enable the ductile–laminate failure mechanism.

The lower interstitial content for LAW HP-LCAC Mo likely enables faster point defect motion to sinks for slightly greater annihilation that results in slightly lower void sizes and void number density, less irradiation hardening, lower change in electrical resistivity, and lower DBTT at lower fluences in comparison to LAW ODS Mo. This is consistent with literature results for unalloyed molybdenum where improved resistance to irradiation effects have been observed with higher purity [28,66], but the improvement with lower interstitial purity observed here for HP-LCAC Mo is relatively slight and the fluences are low.

Acknowledgements

This work was supported under USDOE Contract No. DE-AC11-98PN38206. Thanks to the following ORNL personnel for completing the irradiations, tensile testing, fractography, and TEM (M.M. Li and J.T. Busby). Research at the ORNL SHaRE Use Center was sponsored by the Division of Materials Sciences and Engineering, US Department of Energy. ORNL is managed for DOE by UT-Battelle, LLC, under contract DE-AC-05-00OR22725.

References

[1] J.B. Lambert, J.J. Rausch, Non-Ferrous Alloys and Special-Purpose Materials, Materials Handbook, vol. 2, ASM International, Materials Park, OH, 1992. p. 557.
[2] J. Wadsworth, C.M. Packer, P.M. Chewey, W.C. Coons, Met. Trans. 15A (1984) 1741.
[3] S.J. Zinkle, N.M. Ghoniem, Fusion Eng. Des. 51–52 (2000) 55.
[4] V.K. Sikka, J. Moteff, Nucl. Technol. 22 (1974) 52.
[5] R.E. Gold, D.L. Harrod, J. Nucl. Mater. 85–86 (1979) 805.
[6] B.N. Singh et al., J. Nucl. Mater. 212–215 (1994) 1292.
[7] A. Kumar, B.L. Eyre, Proc. R Soc. Lond. A370 (1980) 431.
[8] H. Kurishita, H. Yoshinaga, Mater. Forum 13 (1989) 161.
[9] W.D. Klopp, J. Less-Common Met. 42 (1975) 261.
[10] A. Lawley, J. Van den Sype, R. Maddin, J. Inst. Met. 91 (1962–1963) 23.
[11] C. Grandhi, M.F. Ashby, Acta Mater. 27 (1979) 1565.
[12] M. Semchyshen, R.Q. Barr, J. Less-Common Met. 11 (1966) 1.
[13] J. Wadsworth, T.G. Nieh, J.J. Stephens, Scripta Mater. 20 (1986) 637.
[14] J.C. Thornley, A.S. Wronski, Acta Mater. 18 (1970) 1053.
[15] A.A. Johnson, S.P. Gupta, S.P. Kodali, Mater. Sci. Eng 18 (1975) 159.
[16] S. Morozumi, in: Proceedings of the Mechanical Properties of bcc Metals, Metallurgical Society/AIME, 1982, p. 197.
[17] G.W. Brock, Trans. Met. Soc. AIME 221 (1961) 1055.
[18] J.B. Brosse, R. Fillit, M. Biscondi, Scripta Mater. 15 (1981) 619.
[19] K. Furuya, J. Moteff, Met. Trans. 12A (July) (1981) 1303.

[20] R. Bianco, R.W. Buckman, Jr., C.B. Geller, High Strength, Creep-Resistant Molybdenum Alloy and Process For Producing the Same, US Patent #5, 868,876, February 9, 1999.
[21] A.J. Mueller, J.A. Shields, R.W. Buckman, Jr., in: G. Kneringer, P. Rodhammer, H. Wildner, (Eds.), Proceedings of 15th International Plansee Seminar, vol. 1, Plansee Holding AG, Reutte, Austria, 2001, p. 485.
[22] R. Bianco, R.W. Buckman, Jr., Evaluation of oxide dispersion strengthened (ODS) molybdenum alloys, in: ASM/TMS Symposium on High Temperature Materials, May 19, 1995, GE CR&D Center, Schenectady, NY (available as WAPD-T-3073, DOE/OSTI, Oak Ridge, TN, 1995).
[23] R. Bianco, R.W. Buckman Jr., in: A. Crowson, E.S. Chen, J.A. Shields, P.R. Subramanian (Eds.), Molybdenum and Molybdenum Alloys, The Minerals, Metals & Materials Society, Warrendale, PA, 1998. p. 125.
[24] B.V. Cockeram, Met. Trans. 33A (2002) 3685.
[25] B.V. Cockeram, Met. Trans. 33A (2005) 1777.
[26] B.V. Cockeram, Mater. Sci. Eng. 418A (2006) 120.
[27] B.V. Cockeram, R.W. Smith, L.L. Snead, J. Nucl. Mater. 346 (2005) 165.
[28] A. Hasegawa et al., J. Nucl. Mater. 233–237 (1996) 565.
[29] B.L. Cox, F.W. Wiffen, J. Nucl. Mater. 85–86 (1979) 901.
[30] F.W. Wiffen, in: R.J. Arsenault (Ed.), Proceedings of the 1973 International Conference on Defects and Defect Clusters in BCC Metals and their Alloys, Nuclear Metallurgy, vol. 18, 1973, p. 176.
[31] B.V. Cockeram, J.L. Hollenbeck, L.L. Snead, J. Nucl. Mater. 324 (2004) 77.
[32] B.V. Cockeram, R.W. Smith, L.L. Snead, J. Nucl. Mater. 346 (2005) 145.
[33] S.J. Zinkle, Y. Matsukawa, J. Nucl. Mater. 329–333 (2004) 88.
[34] M. Eldrup, B.N. Singh, S.J. Zhinkle, T.S. Byun, K. Farrell, J. Nucl. Mater. 307–311 (2002) 912.
[35] B.N. Singh, S.J. Zinkle, J. Nucl. Mater. 217 (1994) 161.
[36] B.N. Singh, S.J. Zinkle, J. Nucl. Mater. 206 (1993) 212.
[37] Standard Specification for Molybdenum and Molybdenum Alloy Plate, Sheet, Strip, and Foil, ASTM B386-97, American Society for Testing and Materials, Philadelphia, PA, 1997.
[38] B.V. Cockeram, J.L. Hollenbeck, L.L. Snead, J. Nucl. Mater. 336 (2005) 299.
[39] L.L. Snead, A.W. Williams, A.L. Qualls, in: M.L. Grossbeck (Ed.), Effects of Radiation Damage on Materials, ASTM STP 1447, ASTM International, West Conshohocken, PA, 2003.
[40] L.R. Greenwood, F.A. Garner, J. Nucl. Mater. 212–215 (1994) 635.
[41] L.R. Greenwood, R.K. Smither, Specter: Neutron Damage Calculations for Materials Irradiations, ANL/FPP/TM-197, Argonne National Laboratory, January, 1985.
[42] Standard Test Methods for Tension Testing of Metallic Materials, ASTM E8-01, American Society for Testing and Materials, Philadelphia, PA, 2001.
[43] Standard Test Method for Resistivity of Electrical Conductor Materials, ASTM B193-96, American Society for Testing and Materials, Philadelphia, PA, 1995.
[44] R. Baranwal, M.G. Burke, Transmission electron microscopy of oxide dispersion strengthened (ODS) molybdenum: effects of irradiation on material structure, in: Proceedings of Microstructural Processes in Irradiated Materials, San Diego, CA, March, 2003, TMS, 2004. (Available as B-T-3462, DOE/OSTI, Oak Ridge, TN, 2003).
[45] T. Diaz de la Rubia, M.W. Guinan, J. Nucl. Mater. 174 (1990) 151.
[46] E. Alonso, M.J. Caturla, T. Diaz de la Rubia, J.M. Perlado, J. Nucl. Mater. 276 (2000) 221.
[47] R.E. Stoller, G.R. Odette, B.D. Wirth, J. Nucl. Mater. 251 (1997) 49.
[48] J.F. Ziegler, J.P. Biersack, U. Littmark, The Stopping and Range of Ions in Matter, Pergamon, New York, 1985.
[49] G. Ackland, V. Vitek, Phys. Rev. B 41 (1990) 10324.
[50] B.D. Wirth, personal communication.
[51] K.S. Chan, Met. Trans. 20A (1989) 155.
[52] K.S. Chan, Met. Trans. 20A (1989) 2337.
[53] K. Watanabe et al., J. Nucl. Mater. 258–263 (1998) 848.
[54] V. Chakin, V. Kazakov, J. Nucl. Mater. 233–237 (1996) 570.
[55] K. Abe et al., J. Nucl. Mater. 122–123 (1984) 671.
[56] K. Abe et al., J. Nucl. Mater. 99 (1981) 25.
[57] M. Scibetta, R. Chaouadi, J.L. Puzzolante, J. Nucl. Mater. 283–287 (2000) 455.
[58] T.H. Webster et al., in: Proceedings of BNES Conference on Irradiation Embrittlement and Creep in Fuel Cladding and Core Components, November 9–10, 1972, p. 61.
[59] I.V. Gorynin et al., J. Nucl. Mater. 191–194 (1992) 421.
[60] A. Hasegawa et al., J. Nucl. Mater. 225 (1995) 259.
[61] H.H. Smith, D.J. Michel, J. Nucl. Mater. 66 (1977) 125.
[62] D.R. Olander, Fundamental Aspects of Nuclear Reactor Fuel Elements, Technical Information Center, US-DOE, ERDA 1976 (TID 2671).
[63] V.K. Sikka, J. Moteff, J. Nucl. Mater. 54 (1974) 325.
[64] J. Moteff, D.J. Michel, V.K. Sikka, The influence of irradiation temperature on the hardening behavior on the refractory BCC metals and alloys, in: R.J. Arsenault (Ed.), Proceedings of the 1973 International Conference on Defects and Defect Clusters in BCC. Metals and their Alloys, Nuclear Metallurgy, vol. 18, 1973, p. 176.
[65] G.E. Lucas, J. Nucl. Mater. 206 (1993) 287.
[66] B.N. Singh et al., J. Nucl. Mater. 223 (1995) 95.
[67] D.S. Gelles et al., J. Nucl. Mater. 103–104 (1981) 1141.
[68] K. Abe et al., Mater. Trans., JIM 34 (1993) 1137.
[69] F.A. Garner, J.F. Stubbins, J. Nucl. Mater. 212–215 (1994) 1298.
[70] J.H. Evans, J. Nucl. Mater. 88 (1980) 31.
[71] J.L. Brimhall, J. Nucl. Mater. 48 (1973) 339.
[72] J. Bentley, PhD Thesis, The University of Birmingham, UK, November 1974.
[73] M. Victoria, N. Baluc, C. Bailat, Y. Dai, M.I. Luppo, R. Ublin, B.N. Singh, J. Nucl. Mater. 276 (2000) 114.
[74] R.W. Smith, Z. Phys. D 21 (1991) 57.